DESIGN OF JOURNAL BEARINGS FOR ROTATING MACHINERY

By

P. E. Allaire

Associate Professor

and

R. D. Flack

Associate Professor

Department of Mechanical and Aerospace Engineering

University of Virginia

Charlottesville, Virginia

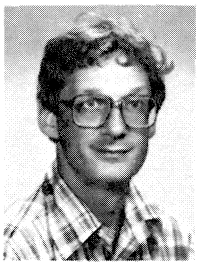

Dr. Paul E. Allaire is currently working on the analysis of flows in pumps, compressors, and turbines. The emphasis is on rotating machinery vibrations caused by these flows. Dr. Allaire has also worked extensively in the area of bearing analysis and finite element analysis. He has developed a number of computer programs for bearings which are widely used in the United States to calculate bearing static and dynamic properties.

Dr. Ronald D. Flack is an associate professor in the Department of Mechanical Engineering at the University of Virginia. His research areas are in experimental bearing lubrication, fluid flows in turbomachines, and rotor dynamics. He has published papers in these areas. He received B.S.M.E., M.S.M.E., and Ph.D. degrees from Purdue University in 1970, 1973 and 1975, respectively, and was employed by Pratt and Whitney Aircraft from 1970 through 1971. He is an active member of ASLE, ASME, ASEE and other societies.

ABSTRACT

Rotating machinery is often subject to vibrations due to critical speeds, unbalance, and instability. Usually the least expensive modification of a machine to make is the bearing. A wide variety of bearings have been developed to combat some of the different types of vibration problems. This paper discusses the geometry and theoretical and experimental results which have been obtained for a number of bearing types. The three main bearing types discussed in this work are multilobe, pressure dam, and tilting pad bearings. A bearing summary chart indicating some of the advantages and disadvantages of these bearing types as well as others is included in the paper.

INTRODUCTION

It is often the case in industry that a rotating machine is designed from the point of view of the pressure to be delivered, the flow rate to be delivered, the torque required of the electric motor, and other factors which are independent of vibration considerations. Near the end of the design process the vibration characteristics of the rotor-bearing system are considered. If vibration problems are encountered either in the design stages or testing stages, it is very difficult to redesign the entire rotor at this point. The easiest change to make is often a bearing change. Thus, the designer and user of rotating machinery should be acquainted with the fundamentals of the vibration suppression characteristics of a number of different fluid film bearings.

Rotating machines are commonly supported in fluid film hydrodynamic bearings. They have relatively low frictional resistance to turning, but more importantly provide viscous damping to reduce lateral vibrations in these machines. If a given machine configuration were supported in rolling element bearings rather than the fluid film bearings, generally the vibration would be so large as to totally prevent operation of the machine due to vibration. Rolling element bearings provide the stiffness necessary to support the weight of the machine but have essentially zero damping or shock absorbing capabilities.

A number of causes of large vibrations in rotating machinery exist. These are described in detail in other references and will only be mentioned here. They include machine unbalance, hydrodynamic journal bearings themselves, interaction with the working fluid in a machine, seals in rotating machines, friction rubs, and internal friction due to stress reversals in shrunk-on parts. Normally, all except the first category, due to machine unbalance, produce a large amplitude of vibration in the machine which occurs at a different frequency from that of the rotating frequency. The resulting dynamic shaft motion, called an instability, occurs at a frequency less than that of the rotating speed and is called subsynchronous vibration. Many of the bearings described in this article have been developed specifically to combat one or another of the causes of instability indicated above. Usually if a bearing has good damping properties such that it will suppress one of the causes of instability, it will also greatly moderate the other causes as well.

A typical vibration pattern for an industrial compressor with vibration problems [1] is shown in the waterfall diagram in Figure 1a. A subsynchronous vibration first occurs at a running speed of 10,800 RPM. The frequency of this whirl motion is near 4000 RPM, which is also the machine first critical speed. At the operating speed of 13,500 RPM, it shows synchronous vibration at 13,500 RPM along the dotted line of 1N RPM, subsynchronous vibration at approximately 4000 RPM, and supersynchronous vibration at 27,000 RPM at 2N. The first value of subsynchronous vibrations is caused by machine seal

forces, internal aerodynamic cross-coupling, and inadequate damping at the bearing stations. This should be eliminated by changing the seal geometry and the bearing stiffness and damping characteristics. The synchronous vibrations at 1N can be improved by a better balancing of the system. Finally, the supersynchronous vibration at 2N can be improved by a better alignment of the compressor to the driving machine.

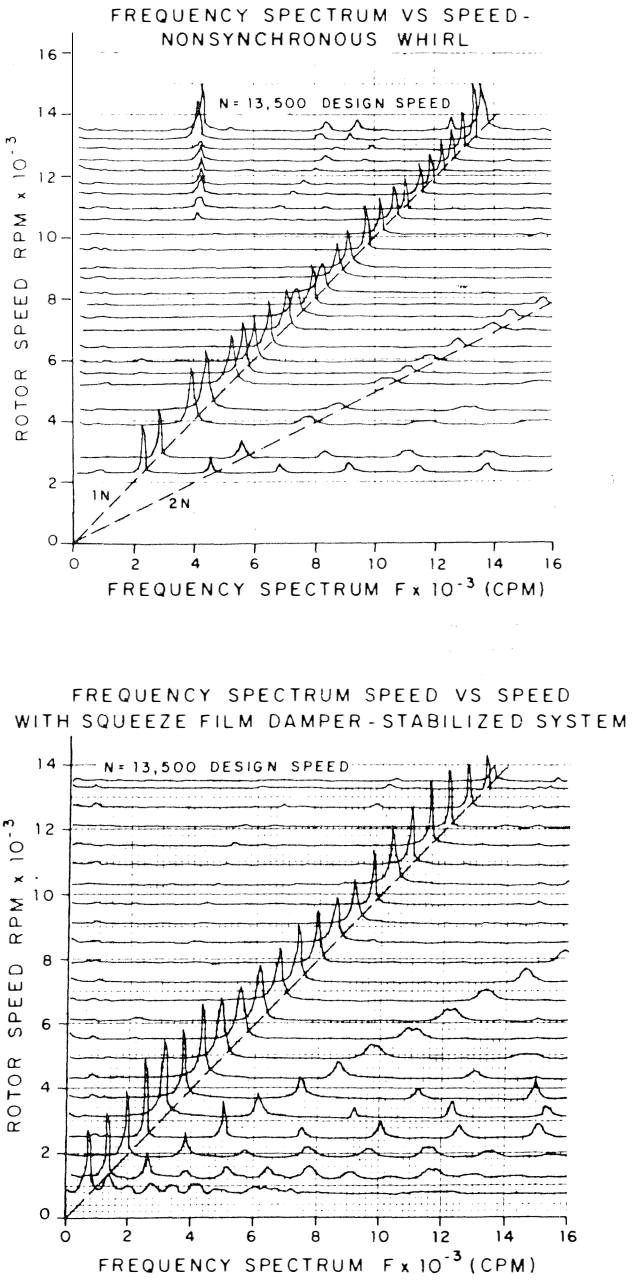

Figure 1. Industrial Compressor with Vibration Problems.
a) Before Fix
b) After Fix

Figure 1b shows that vibration pattern following these improvements except alignment. It can be seen that there is no subsynchronous vibration, a small synchronous vibration, and still the two times supersynchronous vibration. The machine is now running properly and has been for quite some years.

Many of the bearings which are discussed in this paper have been developed principally to combat one or another of the causes of vibration. It is fortunate for designers of rotating machinery that a bearing which has good stiffness and damping properties such that it will suppress one of the causes of vibration will usually moderate one of the others as well. It should be noted, however, that the range of bearing properties due to the different geometric effects is so large that one must be relatively careful to choose the bearing with the property characteristics for the particular causes of vibration for a given machine. In other words, there is no one bearing which will fix every machine.

BEARING TYPES AND GEOMETRY

Fixed Pad Non-Preloaded Journal Bearing

Four types of bearings are shown in Figure 2 which are all somewhat similar to the plain journal bearing. The plain journal bearing has been discussed in great detail elsewhere. Partial arc bearings are a part of a circular arc, as shown in Figure 2b, where a centrally loaded 150° partial arc is presented. If the shaft has radius R, the pad is manufactured with radius R + c. An axial groove bearing, diagrammed in Figure 2c, has axial grooves machined in an otherwise circular bearing. The floating bush bearing has a ring which rotates with some fraction of the shaft angular velocity. All of these are called non-preloaded bearings because the pad surfaces are located on a circle with radius R + c. Preloaded bearings are discussed in detail later in this section.

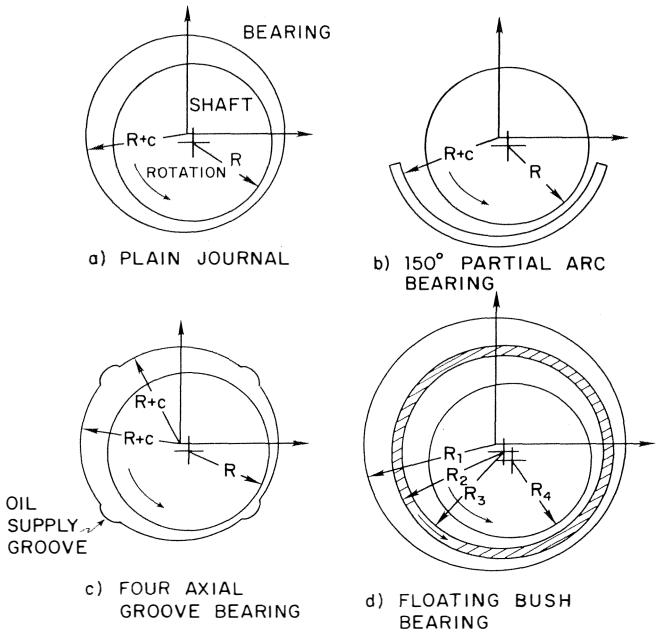

Figure 2. Types of Fixed Pad Non-preloaded Journal Bearings.

Partial arc bearings are only used in relatively low speed applications. They reduce power loss by not having the upper pad, but allow large vertical vibrations. Plain journal and axial groove bearings are rarely perfectly circular in shape. Except in a very few cases, such as large nuclear water pump bearings which are made of carbon, these are crushed in order to make the bearing slightly non-circular. It has been found over many

years of practical use of such bearings that inserting a shim or some other means of decreasing the clearance slightly in the vertical direction makes the machine run much better. Cylindrical plain journal bearings are subject to a phenomenon known as oil whirl, which occurs at half of the operating speed of the bearing. Thus, it is called half-frequency whirl. Axial groove bearings have a number of axial grooves cut in the surface which provide for a better oil supply and also suppress whirl to a relatively small degree. Floating bush bearings reduce the power loss as compared to an equivalent plain journal bearing but are also subject to oil whirl. All of these bearings have the major advantage of being low in cost and easy to make.

Fixed Pad Preloaded Journal bearings

Figure 3 shows elliptical, offset half and three- and four-lobe bearings which are different from the purely cylindrical bearings in that the centers of curvature of each of the pads are not at the same point. Each pad is moved in toward the center of the bearing some fraction of the pad clearance in order to make the fluid film thickness more converging and diverging in nature than occurs in the plain or axial groove journal bearings. The pad center of curvature is indicated by a cross. Generally, these bearings give good suppression of instabilities in the system, but can be subject to subsynchronous vibration at high speeds. Accurate manufacture of these bearings is not always easy to obtain.

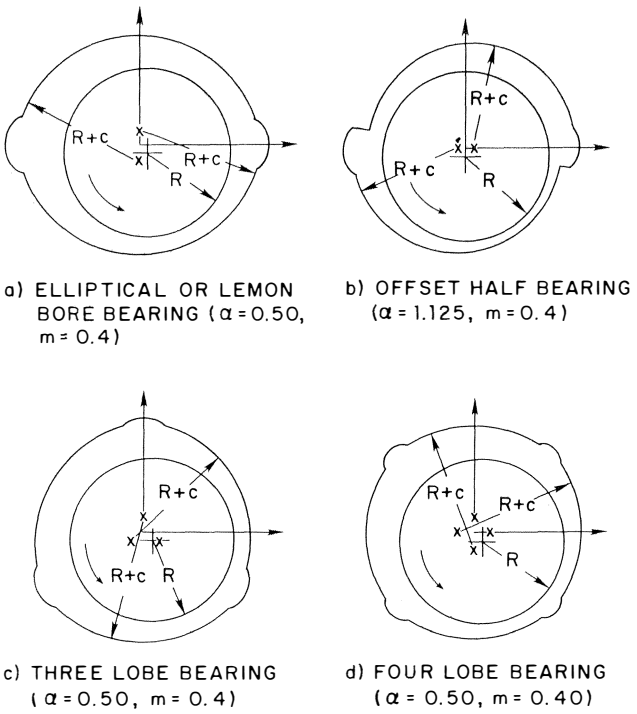

Figure 3. Types of Fixed Pad Preloaded Journal Bearings.

A key parameter used in describing these bearings is the fraction of converging pad to full pad length. Ratio α, called the offset factor, is

$$\text{Offset Factor} = \alpha = \frac{\text{Converging Pad Length}}{\text{Pad Arc Length}}.$$

The elliptical bearing, shown in Figure 3a, indicates that the two pad centers of curvature are moved along the y-axis. This creates a pad which has each film thickness which is one-half converging and one-half diverging (if the shaft were centered) corresponding to an offset factor $\alpha = 0.5$. The offset half bearing in Figure 3b consists of a two-axial groove bearing relative to the bottom half. It has high horizontal stiffness with low vertical stiffness. It is essentially no more difficult to make than the axial groove bearing. Generally, the vibration characteristics of this bearing are such as to avoid the previously mentioned oil whirl which can drive a machine unstable. The offset half bearing has a purely converging pad with pad arc length 160° and the point opposite the center of curvature at 180°. Both the three lobe and four lobe bearings shown have an offset factor of $\alpha = 0.5$.

The fraction of pad clearance which the pads are brought in is called the preload factor, m. Let the bearing clearance at the pad minimum film thickness (with the shaft centered) be denoted by c_b. Figure 4a shows that the largest shaft which can be placed in the bearing has radius $R + c_b$. Then the preload factor m is given by the ratio of $c - c_b$ divided by c,

$$\text{Preload Factor} = m = \frac{c - c_b}{c}.$$

A preload factor of zero corresponds to having all of the pad centers of curvature coincide at the center of the bearing, while a preload factor of 1.0 corresponds to having all of the pads touching the shaft. Figures 4b and 4c illustrate both of these cases where the shaft radius and pad clearance are held constant.

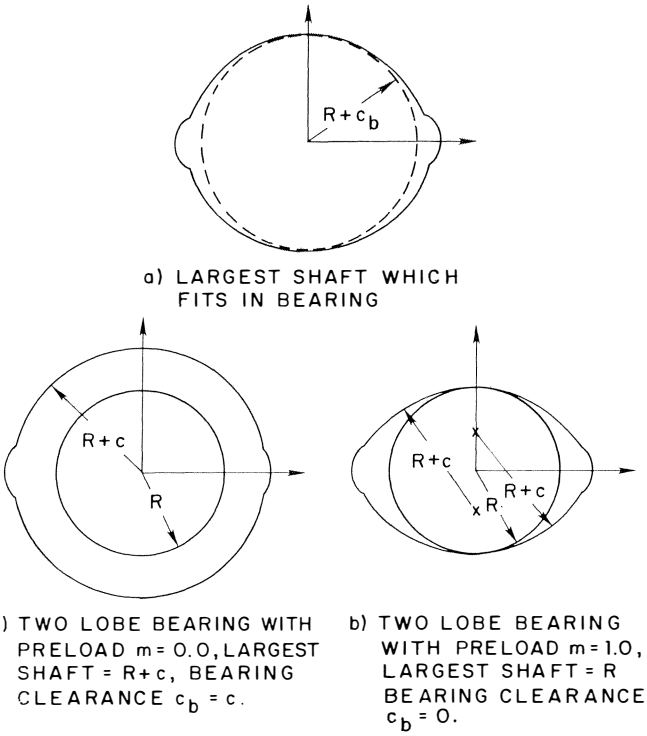

Figure 4. Effect of Preload on Two Lobe Bearing.

Fixed Pad Journal Bearings with Steps, Dams, or Pockets

Pressure dam bearings, shown in Figure 5a, are composed of a plain journal or two axial groove bearing in which a dam is

cut in the top pad. If the dam height is c_d, the radius of the bearing in the dam region is R + c + c_d. As the fluid rotates into the dam region, a large hydrodynamic pressure is created on top of the shaft. The resulting hydrodynamic force adds to the static load on the bearing making the shaft appear to weigh much more than it actually does. This has the effect of making the bearing appear much more heavily loaded and thus more stable. Pressure dam bearings are extremely popular with machines used in the petrochemical industry and are often used for replacement bearings in this industry. It is easy to convert one of the axial groove or elliptical bearing types over to a pressure dam bearing simply by milling out a dam. With proper design of the dam, these bearings can reduce vibration problems in a wide range of machines. Generally, one must have some idea of what the magnitude and direction of the bearing load is to properly design the dam.

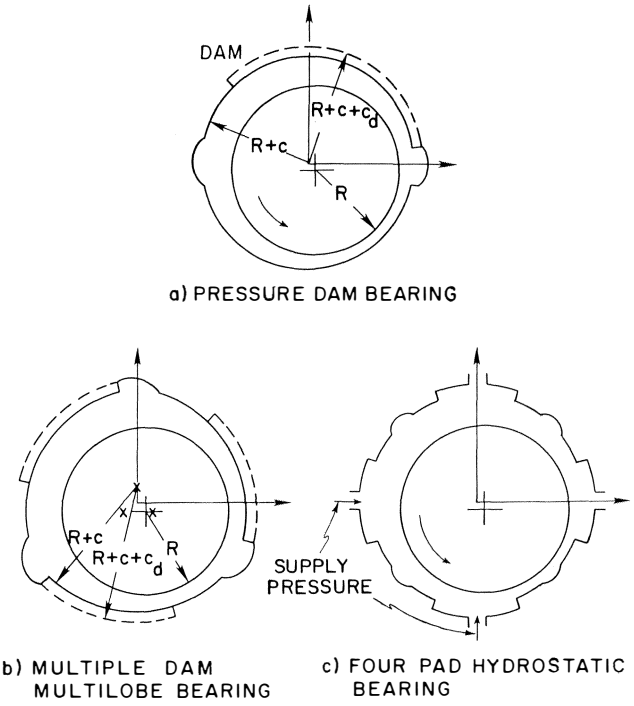

Figure 5. Fixed Pad Journal Bearings with Steps, Dams, or Pockets.

Some manufacturers of rotating machinery have tried to design a single bearing which can be used for all or almost all of their machines in a relatively routine fashion. An example is the multiple axial groove or multilobe bearing shown in Figure 5b. It incorporates a number of features of other bearings which are desirable.

Hydrostatic bearings, shown in Figure 5b, are composed of a set of pockets surrounding the shaft through which a high pressure lubricant is supplied. Clearly, the use of a hydrostatic bearing requires an external supply of high pressure lubricant which may or may not be available on a particular machine. The bearings also tend to be relatively stiff as compared with other hydrodynamic bearings. They are normally used in high precision rotors such as grinding machines or nuclear water pumps for high stiffness.

Non-Fixed Pad Journal Bearings

The last category is the only non-fixed pad journal bearing which is widely used in industry. It is called the tilting pad bearing and each of the pads, which normally vary anywhere from three up to seven, are free to tilt about pivot points indicated in Figure 6. Each pad is pivoted at a point behind the pad which means that there cannot be any moment on the pad. The pad tilts such that its center of curvature, shown in Figure 6b, moves to create a strongly converging pad film thickness. The pivot point is set anywhere from one-half the length of the pad to nearly all the way at the trailing edge of the pad. The fraction of the distance from the leading edge to the pad pivot point divided by the distance from the pad leading edge to the trailing edge is called the offset factor, similar to the offset factor for multilobe bearings. Offset factors vary from 0.5 to 1.0. An offset factor less than 0.5 creates a significant fraction of diverging wedge which is undesirable. If there is any possibility that the bearings will rotate in the direction opposite to the design direction, an offset of 0.5 should be used. An offset of 0.5 also avoids the problem of the pad being installed backwards, which has been known to occur on machines.

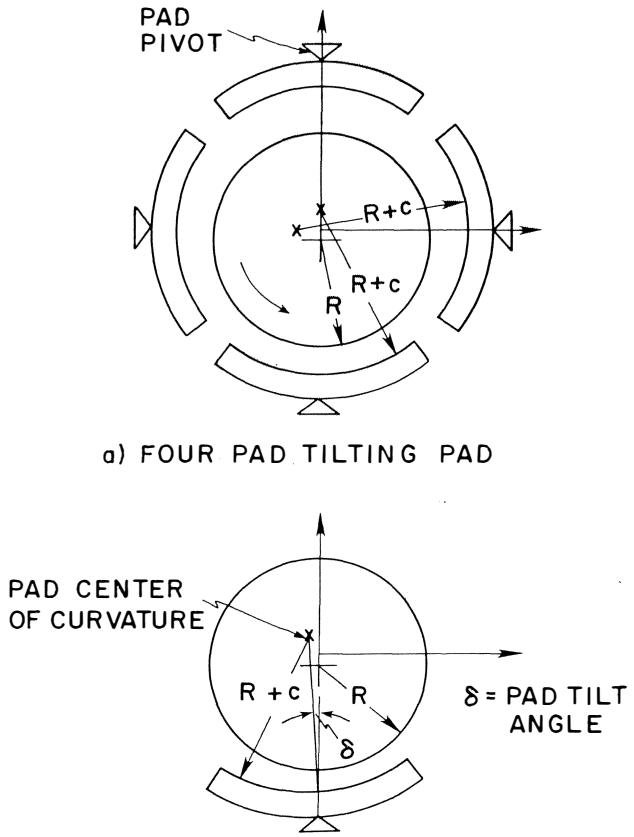

Figure 6. Tilting Pad Bearing Geometry.

Another major design consideration for tilting pad bearings is the radial location of the pad pivot point. It may be moved so that the pad centers of curvature do not coincide at a point at the center of the bearing. This is a preload factor

essentially the same as described above for elliptical and three- and four-lobe bearings. A preload factor less than zero (pad center of curvature between the pad and the bearing center) creates a pad which will tend to dig the leading edge into the shaft. This is sometimes called pad lock-up. Lock-up can be prevented by placing a small bevel on the pad leading edge, which produces a small converging wedge effect, but negative preloads should be avoided.

Tilting pad bearings are very widely used to stabilize machines which have subsynchronous vibrations. Because the pads are free to follow the shaft, the forces produced in the bearing are not capable of driving the shaft in an unstable mode. Their disadvantages include high cost as a retrofit, inability to be retrofitted on some machines, high horsepower loss, and installation problems.

MULTILOBE BEARINGS

In the previous section the geometries of multilobe bearings were described. In this section some typical theoretical and experimental studies, which demonstrate the operating characteristics of multilobe bearings, are present.

Linearized Stability Analysis for Multilobe Bearings

This section investigates the problem of the linear stability and the nonlinear behavior of a single mass rigid rotor [2,3] in the four multilobe bearing configurations shown in Figure 7: (a) an elliptical "lemon" shaped bearing, (b) an offset elliptical bearing, (c) a three-lobe bearing, and (d) a four-lobe bearing. All of the bearings have a length to diameter ratio of 0.5, preload factor and offset factor of 0.5, except the offset bearing for which the offset is 1.0. Stiffness and damping coefficients are given elsewhere and do not give much of a basis for comparing various bearing designs with one another. The linearized stability threshold is often used for this purpose. It should be emphasized that the linearized stability threshold assumes that the rotor is rigid, which is usually not correct. A full rotor stability analysis with both rotor and bearing properties must be conducted for any machine.

Since multilobe bearings do exhibit self-excited whirl vibration under certain speed and loading conditions, the designers are faced with the problem of selecting the bearing which will be the most stable or have the lowest force levels for a given application. Sometimes, bearings are classified as more stable simply because they are stiffer. A typical instability takes the form of half-frequency whirl occurring at a shaft rotational speed of approximately two times the resonant frequency of a rotor system. The stiffer bearing is designated "more stable" because bearing stiffness increases the natural frequency which effectively raises the stability threshold speed at which bearing induced whirl will occur. In this study, all the bearings are oriented with the weight of the journal directly on the center of the bottom lobe. The ambient and cavitation pressures are taken to be zero. Film rupture is assumed to occur for negative pressures (the half Sommerfeld condition). The Reynolds equation is solved with the pressure at the leading and trailing edge of each bearing sector as well as on the sides assumed to be zero. The hydrodynamic pressure is integrated only over the region in which the pressure is positive.

The equations that lead to the determination of the bearing linearized stability for a rigid rotor are presented in [2]. Figure 8 shows the stability threshold speed ω plotted against the Sommerfeld number for the four bearing types shown in Figure 7. Each of the 45° straight lines with positive slope and constant η across the figures gives the locus of the operation of a bearing with a fixed geometry as it is brought up or down in speed. The bearing parameter η is defined as

$$\eta = \frac{S}{\bar{\omega}_j} = \frac{\mu LD}{8\pi W} \left(\frac{D}{c}\right)^2 \left(\frac{W}{cm}\right)^{1/2}.$$

It should be noted that η is independent of the rotor speed and is in itself sufficient for the description of a certain bearing geometry on a stability graph. As a bearing increases in speed, it will proceed along a line of constant η and become unstable as it enters the unstable region by crossing the stability curve from below.

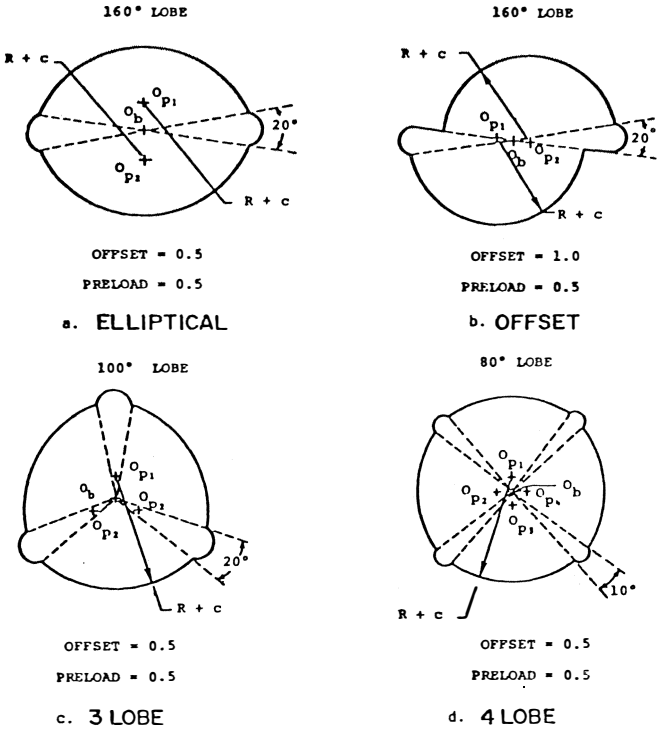

Figure 7. Multilobe Bearing Geometry.

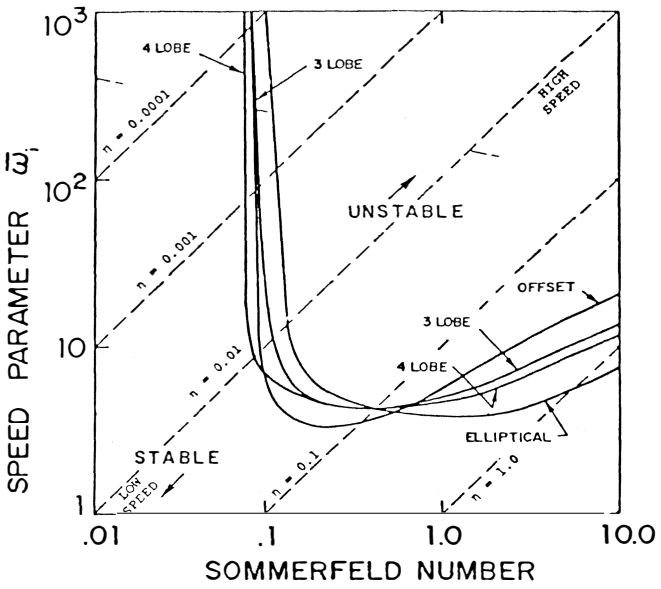

Figure 8. Linearized Bearing Stability for a Rigid Rotor.

Figure 8 may be separated roughly into three regions: light load and/or close clearance (η = 0.1 to 1.0), moderate load and/or moderate clearance (η = 0.01 to 0.1), and heavy load and/or open clearance (η = 0.001 to 0.01). It is observed that under all operating conditions, the three-lobe bearing is consistently more stable than the four-lobe bearing, except at η = 0.1 where the bearings have about the same stability threshold. All the other stability curves also appear to intersect roughly at this same point indicating little difference between the stability characteristics of the bearings in this area of operation.

At light load and/or close clearance operations, the offset bearing is the most stable. The three-lobe bearing is better than the four-lobe bearing by a small margin, while the elliptical "lemon" bearing is the least desirable. Within this region, the stability may be much improved by reducing the lobe clearance or effectively increasing the bearing parameter η.

Under moderate load conditions, the offset half bearing loses its superiority completely. The most stable bearing in this region is the elliptical bearing, followed by the three-lobe, the four-lobe, and the offset cylindrical bearing. Improvement in the stability performance by increasing lobe clearance or decreasing η is not substantial on the high η side within this region.

At heavy load and/or open clearance operations, the order of increasing stability is: the four-lobe bearing, the offset bearing, the three-lobe bearings, and the elliptical bearing. Increasing lobe clearance or decreasing η will drastically improve the stability threshold for all of the bearings.

While the offset bearing is superior in stability for light load operation, the elliptical bearing appears to be most stable for a wide range from heavy loaded to relatively lightly loaded applications.

Although the three-lobe bearing does not have the best stability, it offers good overall performance under all load conditions. It is second only to the most stable bearing in each region.

The ratio of the whirl speed to the rotor speed is given by the dimensionless imaginary part of the unstable complex eigenvalues [2]. At the stability threshold, the real part of the root is zero, and the whirl ratio, $\bar{\omega}_d$, may conveniently be computed.

Figure 9 shows the variation of the whirl ratio with the Sommerfeld number for the four bearing types at the threshold of instability. It is seen that a definite relation exists between the stability and the whirl ratio in a way that the more stable bearing distinctly whirls at a lower speed ratio.

With the exception of the elliptical bearing, all bearings whirl at speeds less than 0.48 of the rotor speed. The offset bearing attains a maximum whirl ratio of 0.44 at a Sommerfeld number of about 0.4 and decreases to a steady value of 0.35 at higher Sommerfeld numbers. This observation corresponds to the superior stability with the offset bearing at high speed and light load operations.

The whirl ratios with the three-lobe and the four-lobe bearings share similar characteristics. They both rise sharply at low Sommerfeld numbers and remain fairly constant for most portions of the curves. Asymptotic whirl ratios of 0.47 and 0.48, respectively, are reached at high Sommerfeld numbers. In comparison to the four-lobe bearing, the three-lobe bearing always has the lower whirl ratio.

The elliptical bearing which is the least desirable for lightly loaded applications is seen to have a whirl ratio in excess of 0.5 above a Sommerfeld number of 1.3. Whirl ratios above 0.5 have been observed by other authors as well. The highest

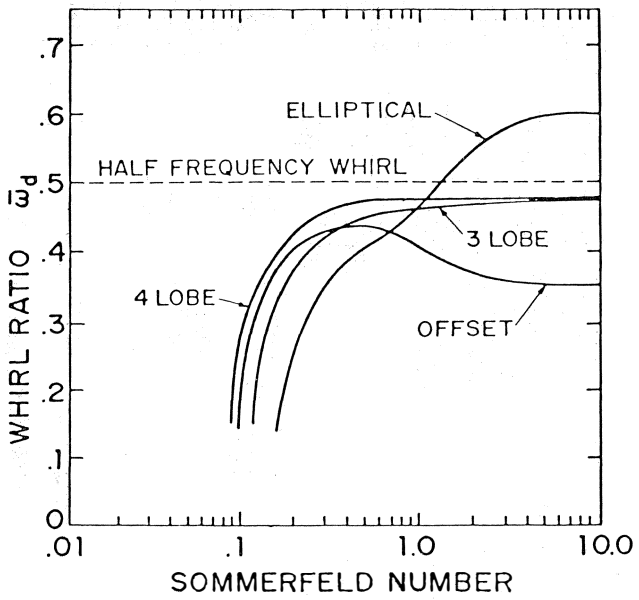

Figure 9. Whirl Speed Ratio Versus Sommerfeld Number.

whirl ratio of 0.6 is reached asymptotically at high Sommerfeld numbers.

All the curves in Figure 9 drop very rapidly when the bearings are operated near the steep vertical region of the stability curves. When a bearing is infinitely stable, the whirl ratio approaches zero.

Using a single mass flexible rotor, it can be shown that the flexible rotor stability threshold is given by [2]

$$\bar{\bar{\omega}}_s = \frac{\bar{\omega}_s}{1 + \bar{\omega}_s^2\, \bar{\omega}_d^2 \left(\dfrac{g}{c\omega_r^2}\right)^{1/2}},$$

where ω_r is the rotor critical speed on rigid bearings. Because the stability threshold for a flexible rotor is always lower than that for a rigid rotor, Figure 9 should be viewed as the highest possible stability that can be achieved in these bearings.

One of the major concerns in this investigation is the stability of the multilobe bearings in light load applications. The non-linear characteristic of the bearings examined in this section are to have the bearing parameter η = 0.3. Insofar as possible, generalization of the results throughout this paper is provided by the use of dimensionless parameters instead of particular bearing specifications and operating conditions. An example bearing with η = 0.3 is

L = 38.1 mm (1.5 in)
D = 76.2 mm (3.0 in)
c = 0.152 mm (0.006 in)
W = 168.3 N (37.8 lb)
μ = 6.89×10^{-3} N−s/m^2 (1.0×10^6 lb−s/in^2).

For comparison to the transient analysis, the linear stability thresholds, corresponding Sommerfeld numbers, and whirl speed ratios for the four bearing types at η = 0.3 are tabulated in Table 1. The journal speeds for each of the four bearing types at the threshold speeds of instability are also shown. The order of increasing stability is the elliptical bearing, the four-lobe bearing, the three-lobe bearing, and the offset bearing.

TABLE 1. STABILITY THRESHOLDS AND WHIRL RATIOS FOR VARIOUS BEARING TYPES WITH BEARING PARAMETER $\eta = 0.3$.

Bearing Type	Sommerfeld Number S	Whirl Ratio $\bar{\omega}_d$	Stability Threshold $\bar{\omega}_s$	Bearing ω_s(RPM)
Elliptical	1.15	.495	3.82	9,252
4-Lobe	1.52	.475	5.08	12,304
3-Lobe	1.86	.470	6.21	15,041
Offset	3.62	.361	12.07	29,234

Four-Lobe Bearings on a Single Mass Flexible Rotor

In this section, a flexible rotor, described in Appendix A, was mounted in a set of four-lobe bearings. A typical four-lobe bearing is shown in Figure 10. Dynamic behavior and the instability threshold was investigated from several configurations (for more details see reference [4]). All parameters were held constant for all tests with the exception of the value of the load angle θ_g. For a four-lobe bearing, $\theta_g = \gamma_g$. Small changes in this parameter were seen to change the dynamic response considerably. The specifications of the two bearings are summarized in Table 2. The same two bearings were used for all of the tests in this section.

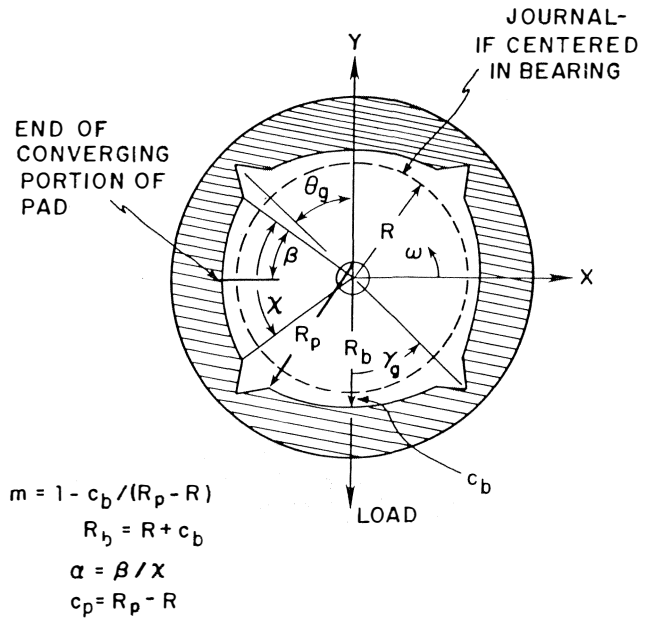

Figure 10. Typical Four-Lobe Bearing.

TABLE 2. FOUR-LOBE BEARING SPECIFICATIONS.

Shaft Diameter (mm)	25.377/25.342*
Minimum Radial Clearance, Cb(mm)	0.041/0.058
Preload Factor, m	0.77/0.70
Pad Angle, χ	63°/63°
Bearing Length, L (mm)	14.22/14.22
Offset Factor, α	0.50/0.50

* Double values indicate left and right bearings, respectively.

The first orientation to be discussed is $\theta_g = -15°$. Figure 11 shows the synchronous motion, total motion, and phase angle responses for rotor run-up for the X2 probe. In this figure, the two most important features are the responses at the rotor first critical speed and at high speeds. First, the rotor is seen to remain stable for all speeds. The maximum speed that the rotor was run was approximately 12,500 RPM and neither the total nor synchronous motion of the rotor displayed any large limit cycle vibration. The overall motion did, however, gradually tend to increase as the speed increased above 6000 RPM. Second, the motion of the rotor at the critical speed is seen to increase.

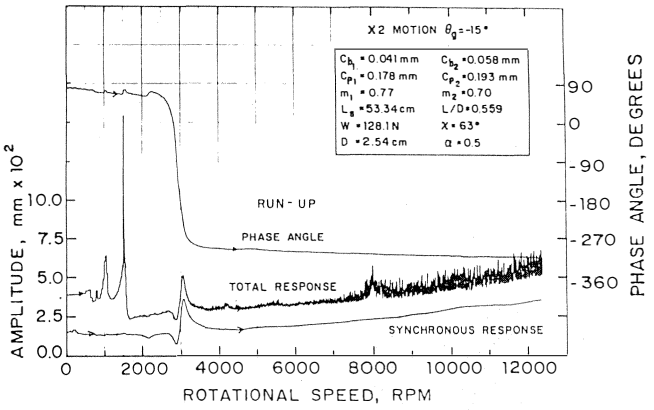

Figure 11. Total and Synchronous X2 Motion (Run-up) for $\theta_g = -15°$.

The classic phase shift observed at a critical speed is 180°. However, an overall phase shift of 360° was observed at X2. This phase shift behavior is attributed to the bow of the rotor.

The waterfall frequency spectrums are presented for the X2 motion in Figure 12. Such a figure complements the synchronous response plots well. For example, the supersynchronous excitation of the rotor critical speed can easily be seen. Also the 2x and 3x components that contribute to the total observed motion can easily be seen. For rotational speeds greater than 6000 RPM the synchronous X2 motion is seen to increase with speed, as was also seen in Figure 11. Lastly, no subsynchronous motion was seen at any time in the operation range. This rotor-bearing system was thus very stable throughout this test.

The second configuration discussed is $\theta_g = 30°$. The X2 total and synchronous motion and phase angle responses are presented for rotor run-up in Figure 13. The rotor went unstable very rapidly at 6600 RPM, as indicated by the total

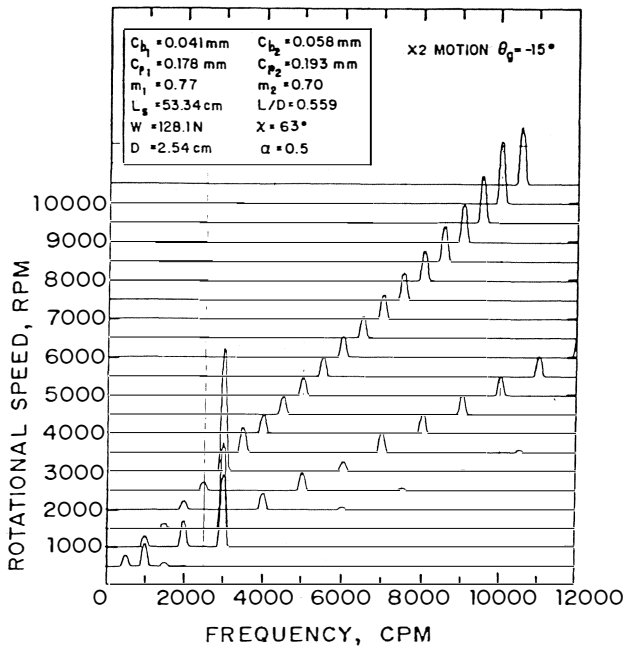

Figure 12. Waterfall Frequency Spectrum X2 Motion for $\theta_g = -15°$.

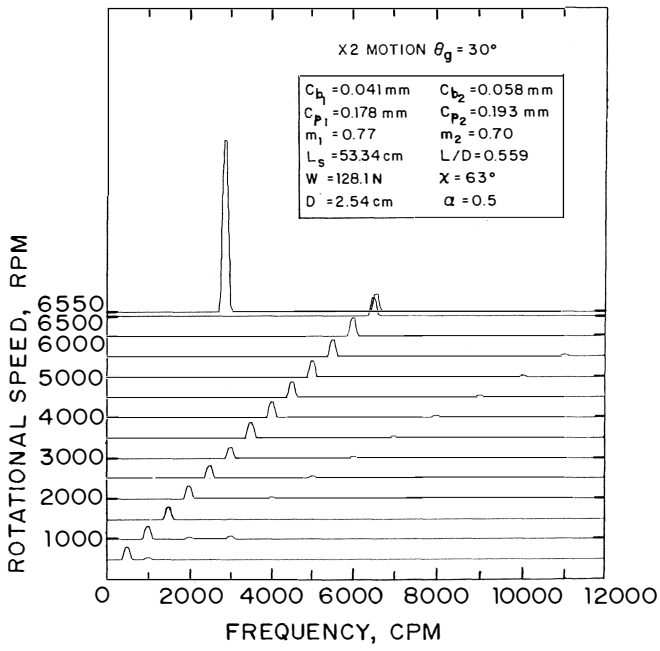

Figure 14. Waterfall Frequency Spectrum for X2 Motion for $\theta_g = 30°$.

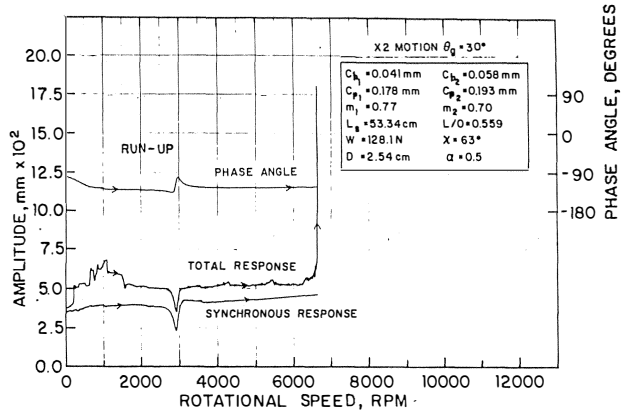

Figure 13. Total and Synchronous X2 Motion (Run-up) for $\theta_g = 30°$.

motion. Thus, rotating the bearings 45° from the initial position reduced the stability threshold by no more than 5900 RPM. On rundown the rotor was locked in an unstable condition, as was also observed for pressure dam bearings.

The waterfall frequency spectrum for $\theta_g = 30°$ (X2 motion, run-up) is presented in Figure 14. This figure is presented to demonstrate the frequency at which the rotor was vibrating during the unstable condition. This frequency is the same as the critical speed of the rotor (approximately 3000 RPM). Other configurations which became unstable also oscillated at this same frequency and the rotor was never seen to demonstrate any half frequency oil whirl. Thus, when this rotor-bearing system demonstrated any instabilities, the condition was whip as opposed to whirl.

Using the results presented above and the results from other tests, the instability threshold speed was correlated with the angular position of the groove (γ_g). This plot is presented in Figure 15. Also plotted in Figure 15 is the end of the hysteretic effect of whip run-down. As can be seen from this figure, the optimum location of the grooves is for a value of γ_g from $-15°$ to 0°, or from 75° to 90°. The worst case is when $\gamma_g = 30°$. On the other hand, the end of whip on run-down is not seen to be a strong function of γ_g. This level remained between 5800 and 7400 RPM for all cases when the system went unstable. This implies that the higher the rotor instability threshold, the longer the rotor will demonstrate whip during run-down. This observation was also made for pressure dam bearings.

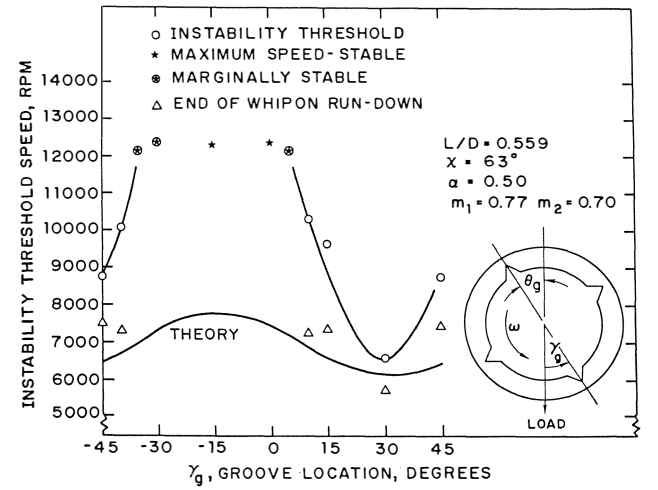

Figure 15. Summary of Correlation of Instability Threshold Speed with γ_g.

The experimental data is next correlated with theoretical predictions. For this section, finite elements were utilized to calculate the bearing coefficients for the four-lobe bearings used here. Also, the flexible rotor was modeled using lumped rotor masses [5]. This model was then used with the bearing coefficients to predict the stability of the rotor-bearing system. This stability threshold was calculated for various values of γ_g and the theoretical predictions are presented in Figure 15. As can be seen, significant differences exist between the experimental data and theoretical predictions for the instability threshold ranging from 400 RPM at $\gamma_g = 30°$ to over 4900 RPM at $\gamma_g = 0°$. Nonetheless, the experimental and theoretical results are in semi-quantitative agreement since the optimum value of γ_g is the same for both ($\gamma_g = -15°$ or 75°).

The differences between the theoretical and experimental instability thresholds for all bearing types are attributed to one or a combination of five effects. The relative magnitudes of these have not been determined. They are: (1) inaccurate boundary conditions (either half Sommerfeld or Reynolds) in the bearing calculations; (2) variations of temperature and, thus, viscosity within the fluid film of the bearings; (3) small orbital motions of the shaft within the bearings resulting in transient variations of the stiffness and damping bearing characteristics; (4) viscoelastic effects of the multigrade oil; and (5) reduced inertia effects of the disks due to damping in the shaft/disk mounts. Studies are presently being planned to partially explain the differences. The shaft is being instrumented such that pressures within the bearing can be measured and compared to theoretical predictions to determine the accuracy of the fluid film bearing boundary conditions.

Two Axial Groove Bearings on a Three Mass Flexible Rotor

Axial groove bearings have been tested in a three mass flexible rotor in a similar manner to the studies done in the previous subsection [6]. The apparatus is similar to the single mass flexible rotor and is described in Appendix B. The specifications of the bearings are presented in Table 3. For brevity, only the summary graph is presented here (Figure 16). As can be seen, the instability threshold is considerably lower for these bearings than for the four-lobe bearings in the single mass rotor. There are two reasons for this. First and most importantly, the preload for these bearings is zero. Second, this apparatus is more flexible due to the smaller shaft diameter. The instability threshold does vary with the load angle and the optimum value of γ_g is once again approximately 75°.

TABLE 3. TWO AXIAL GROOVE BEARINGS.

Shaft Diameter, D (mm)	25.397/25.387
Clearance, c (mm)	0.037/0.042
Pad Angle, χ	151°/151°
Length, L (mm)	12.70/12.70
Preload, m	0.00/0.00

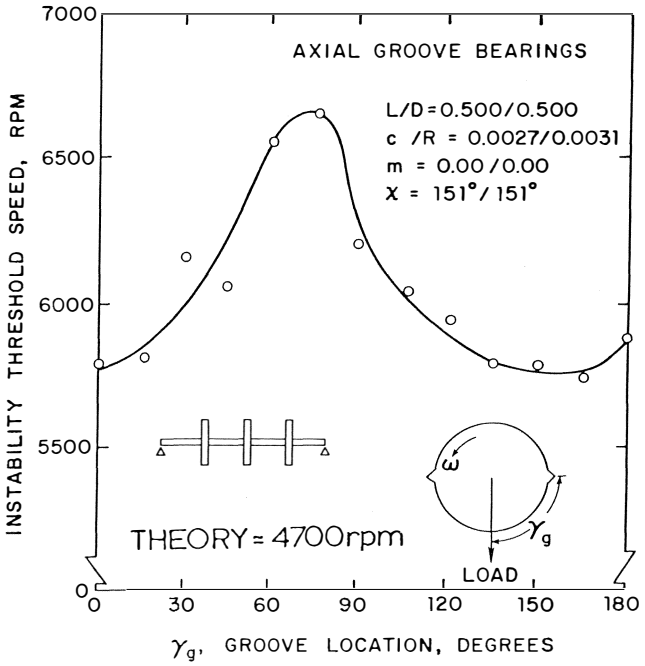

Figure 16. Summary of Correlation of Instability Threshold Speed with γ_g.

For this system the theoretical instability threshold was approximately 4700 RPM, regardless of load angle. The differences between theory and experiment are attributed to the five reasons discussed above.

Three-Lobe Bearings on a Three Mass Flexible Rotor

Seven sets of three-lobe bearings have been tested in the same three mass rotor as described in Appendix B [7]. The specifications are described in Table 4 and the variables are the same as defined for a four-lobe bearing. As can be seen the preload factor and offset factor were systematically varied.

Typical summary plots are presented for three bearing sets in Figures 17 through 19. The summary diagram for set 2 ($\alpha = 0.50$, $m \simeq 0.42$) in Figure 17 shows the experimental instability threshold, which varied from 63.50 RPM at $\gamma_g = 90°$ to 7500 RPM at $\gamma_g = 30°$. Theory shows a minimum instability of 4600 RPM at $\gamma_g = 90°$ and increases up to 5500 RPM at $\gamma_g = 30°$. Although the magnitudes of the instability thresholds are not the same, the experimental data follow the theoretical trends.

TABLE 4. BEARING SPECIFICATIONS.

Set No.	2	3	4	5	6	7	8
Minimum Radial Clearance, c_b (mm)	0.034/0.043	0.034/0.043	0.038/0.043	0.038/0.043	0.038/0.046	0.038/0.043	0.038/0.046
Preload, m	0.0449/0.393	0.595/0.561	0.756/0.732	0.747/0.723	0.766/0.732	0.747/0.723	0.766/0.732
Offset Factor, α	0.500/0.500	0.505/0.505	0.484/0.484	0.677/0.677	0.909/0.909	0.323/0.323	0.091/0.091
Pad Angle, χ	96°/96°	93°/93°	95°/95°	96°/96°	99°/99°	96°/96°	99°/99°

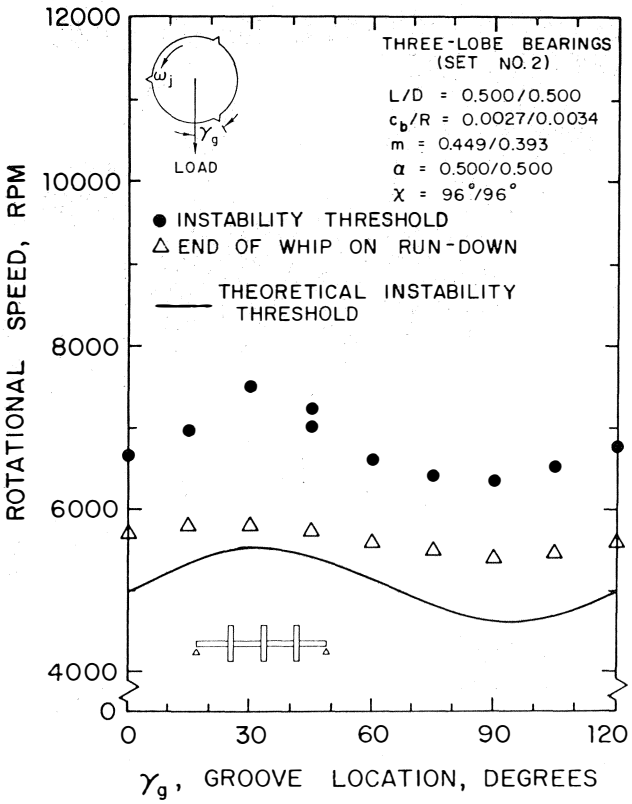

Figure 17. Summary of Instability Threshold and End of Whip Cycle with γ_g for Bearing Set 2.

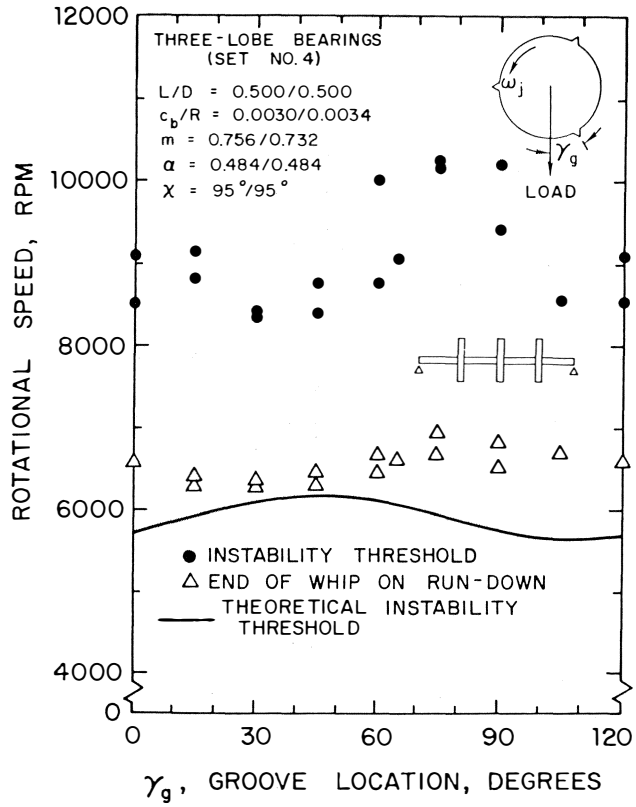

Figure 18. Summary of Instability Threshold and End of Whip Cycle with γ_g for Bearing Set 4.

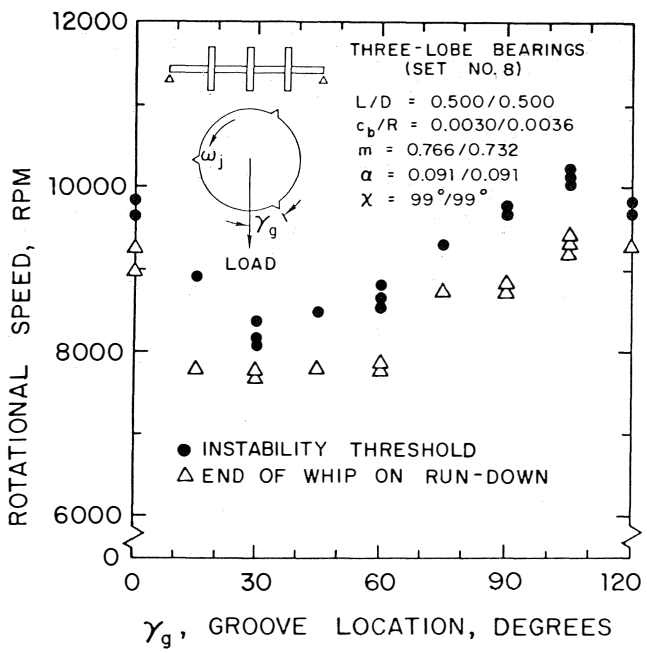

Figure 19. Summary of Instability Threshold and End of Whip Cycle with γ_g for Bearing Set 8.

Set 4 ($\alpha = 0.48$, $m \simeq 0.74$) results are presented in Figure 18. The minimum and maximum instability thresholds were 8400 RPM and 10,250 RPM, respectively, and occurred at $\gamma_g = 30°$ and 75°, respectively. These were the same for both variations of γ_g from 0° to 120° and 120° to 240°, indicating the repeatability of the data. Some scatter does exist for other load orientations. For example, for load angles of 60° and 90°, the instability threshold varied by as much as 1250 RPM depending on the particular pad orientation (e.g., 60° or 180°, etc.). Thus, the pads are not exactly symmetric, as also evidenced by the surface profiles. Theory shows a variance of only 450 RPM from the minimum instability threshold of 5700 RPM at $\gamma_g = 1.05°$ to the maximum instability threshold of 6150 RPM at $\gamma_g = 45°$.

Set 8 ($\alpha \simeq 0.09$., m = 0.75, Figure 19) had instability thresholds which varied from 8200 RPM at $\gamma_g = 30°$ to 10,150 RPM at $\gamma_g = 105°$. For this set of bearings, theoretical predictions are not presented. For large eccentricity ratios, difficulties arose in the convergence of the finite element method. These difficulties were pronounced for small offset factors since the converging fluid-film wedge occurred for only a small portion of each pad (less than ten percent). For large Sommerfeld numbers (as in reference [8]), the method converged. However, for rotational speeds up to 10,000 RPM, the method did not converge.

By comparing theory and experiment in Figures 17 and 18 and for other three-lobe bearings one finds that excellent agreement is not found for any of the conditions. Moderate-to-poor agreement has also been reported for four-lobe bearings in the single-mass flexible rotor. For comparison, good agreement (20 percent and less difference) was found for a single-mass rotor in five different sets of pressure-dam bearings [9]. Also, good agreement (16 percent difference) was found for a three-mass rotor in one set of pressure-dam bearings [6]. Thus, the large differences seen here (up to 45 percent) appear to be partially attributable to the particular bearing type studied here, since good agreement was found for another bearing type. This indicates that the differences are attribut-

able to inaccurate bearing calculations rather than inaccurate rotor modeling. In reference [10], the authors found that neither the half-Sommerfeld nor Reynolds boundary condition predicted pressure profiles which were in good agreement with experimental measurements. Flack and Allaire [11] found that experimental operating eccentricities for three-lobe bearings were lower (by as much as 63 percent) than predicted. The differences between the theoretical and experimental instability thresholds for all bearing types are attributed to a combination of five effects described earlier in this paper.

To summarize the experimental behavior of the instability threshold variation with preload factor and offset factor, Figures 20 and 21 are presented. Figure 20 shows the dependence of the experimental instability threshold at the optimum load angle for bearing sets 2 through 4 versus the preload factor with an offset factor, $\alpha \simeq 0.5$. This figure shows the maximum instability threshold increasing from 6700 RPM with m = 0.0 (two axial groove) to 7500 RPM with m = 0.449/0.393 (3-lobe, set 2), to 10,250 RPM with m = 0.756/0.732 (set 4).

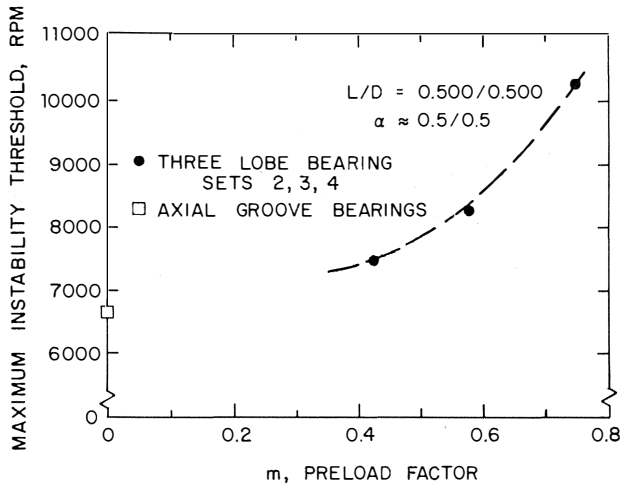

Figure 20. Experimental Summary of Instability Threshold at Optimum Load Angle with Preload Factor.

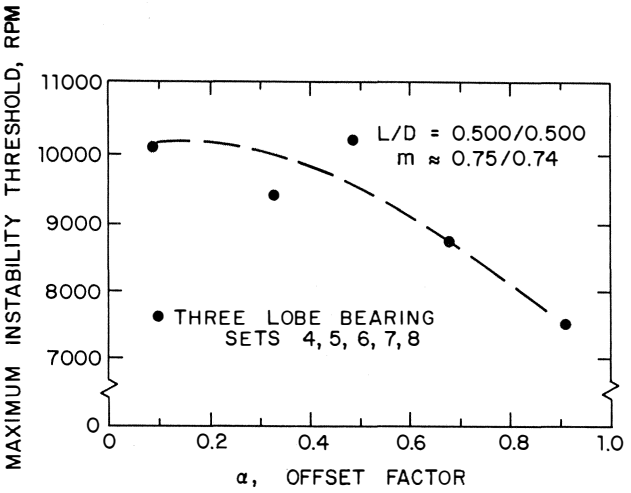

Figure 21. Experimental Summary of Instability Threshold at Optimum Load Angle with Offset Factor.

Figure 21 shows the dependence of the maximum experimental instability threshold versus α with $m \simeq 0.75$. The maximum instability threshold was 10,250 RPM with $\alpha = 0.48$ (set 4) and varied down to 7500 RPM with $\alpha = 0.91$ (set 6).

From the results in Figure 21 the bearings with the smallest offset factors produce the most stable system. However, the bearings in this system were lightly loaded. Because of the small resulting positive pressure regions in bearings with the offset factors less than 0.5, the load carrying capacities are small. As a result, if high loads are applied the bearings may fail prematurely. For the lightly loaded system described here, the bearings operated without problems. However, using such bearings for a heavily loaded system is not recommended.

PRESSURE DAM BEARINGS

Lineralized Stability Analysis for Step Bearings

Pressure dam or step journal bearings have long been used to improve the stability of rotating machinery. They can replace plain journal or axial groove bearings in a machine operating at high speeds and increase the stability threshold. A step or dam is cut in the upper half surface of the bearing producing a pressure rise near the step and a hydrodynamic load on the journal.

At high speeds and/or light loads, the step creates a loading that maintains a minimum operating eccentricity. That is, as speed is increased, the bearing eccentricity does not approach zero as it would for plain journal or two axial groove bearings. The eccentricity approaches some minimum value or may even increase with increasing speed due to the step loading. Thus, a properly designed step bearing would operate at a moderate eccentricity even at high Sommerfeld numbers [12,13,14].

Consider a finite length step bearing as shown in Figures 22 and 23. Many industrial bearings have two oil supply grooves in the horizontal plane and a step located in the second quadrant with counterclockwise shaft rotation. A rectangular

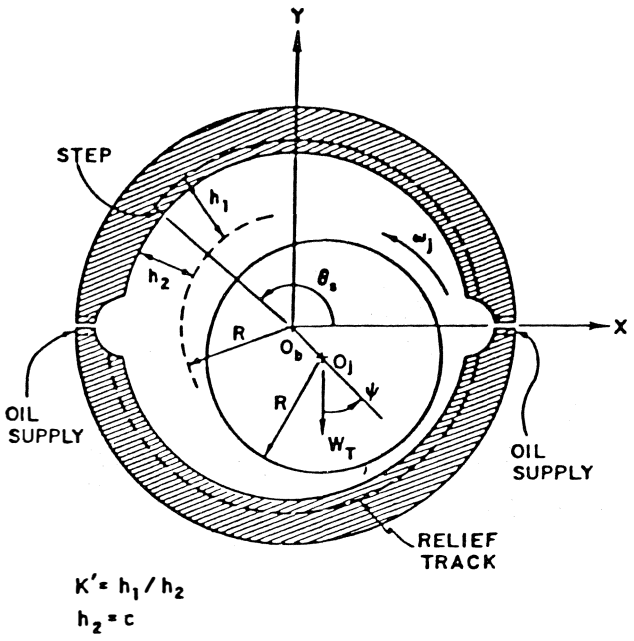

Figure 22. Pressure Dam Schematic Side View.

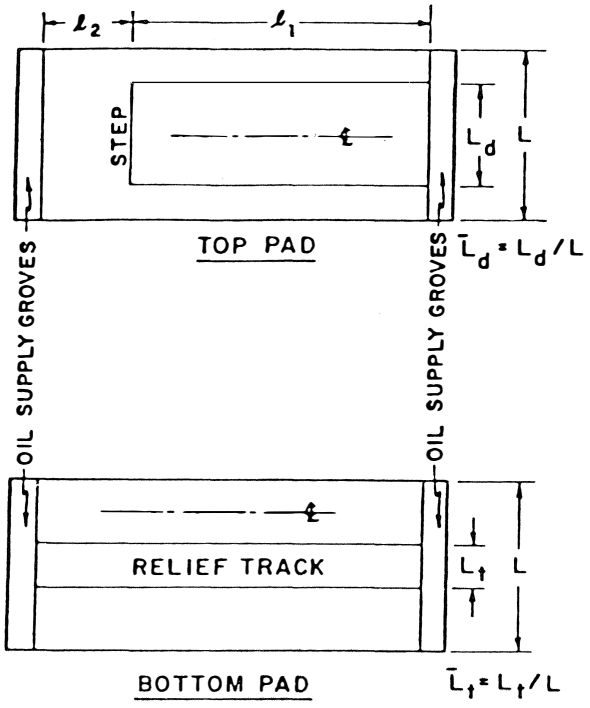

Figure 23. Pressure Dam Schematic, Top and Bottom Pads.

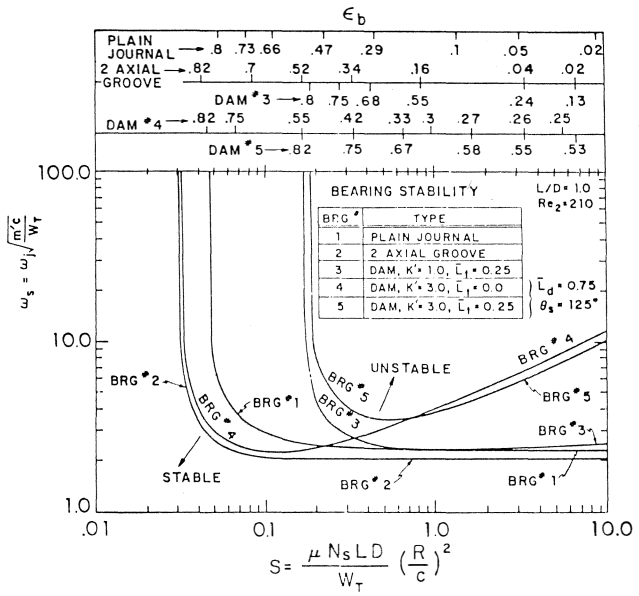

Figure 24. Stability Map Comparing Pressure Dam Bearings to Plain Journal and Two Axial Groove Bearings.

dam is usually used. A circumferential relief groove or track is sometimes grooved in the bottom half of the bearing. Both of these effects (dam and relief track) combine to increase the operating eccentricity of the bearing when compared to a plain journal or two axial groove bearing.

Many geometric variables affect the performance of pressure dam bearings. For all of the step journal bearings analysis in this paper, two 20° oil inlet grooves were located at $\theta = 0°$ and $\theta = 180°$. Also, the dam axial length ratio was held constant at $\bar{L}_d = 0.75$ for all cases. To study the effects of the remaining variables, only one was changed while the others remain the same. Other parameters include:

$L/D = 1.0$
$Re_2 = 210$
$\theta_s = 125°$
$K' = 3.0$
$L_t = 0.25$

This section analyzes the finite length pressure dam bearing neglecting step inertia effects, but including the effects of turbulence over the entire bearing surface. Bearing stability threshold curves for various pressure dam bearing geometries are compared to plain journal, two axial groove and grooved lower half bearings. The effects on the stability threshold of film thickness ratio, dam location, and other geometric parameters are considered. Optimum bearing designs are suggested to provide favorable stability characteristics.

Figure 24 compares the stability characteristics of the plain journal, two axial groove and grooved lower half bearings to two types of pressure dam bearings. The stability threshold speed ,ω_s, is plotted against the Sommerfeld number, S. Also indicated at the top is the bearing eccentricity ratio, ε_b, for all groove bearings, respectively. Note that at high Sommerfeld numbers the stability curves for each bearing approach asymptotic values of $\omega_s = 2.3$ (plain journal) and $\omega_s = 2.05$ (two axial groove).

Bearing number 3 is the grooved lower half bearing. This bearing is simply a two axial groove bearing with a circumferential relief track or groove cut in the lower half. In this case, the relief track axial length ratio (Figure 23) is $\bar{L}_t = 0.25$ (the relief track is 25% of the bottom pad). A considerable increase in the infinite stability region is evident. That is, the plain journal bearing is theoretically stable at all speeds below a Sommerfeld number of 0.48, while the grooved lower half bearing increases this range of infinite stability by a factor of three to $S \leq 0.17$. The relief track removes part of the bearing load carrying surface for the bottom pad, thereby allowing bearing number 3 to reach 0.8 eccentricity at a higher Sommerfeld number than the plain journal bearing. Around $\varepsilon_b = 0.8$, $\bar{K}_{xy}$ changes sign, providing the favorable stability characteristics. Essentially no increase in stability is seen at high Sommerfeld numbers.

Bearing number 4 is a pressure dam bearing with $K' = 3.0$ (dam clearance three times as large as the bearing clearance) and $L_t = 0.0$ (no relief track). For this case, the stability is increased compared to the journal bearing at high Sommerfeld numbers while the region of infinite stability is less. As discussed earlier, at high Sommerfeld numbers the step forces the journal to operate at a moderate eccentricity. From the top of Figure 24 bearing number 4 operates at an eccentricity ratio of $\varepsilon_b = 0.25$ at $S = 5.5$. This moderate eccentricity provides the favorable stability characteristics at high Sommerfeld numbers for this step journal bearing.

Combining the two effects of a relief groove in the lower half and a step in the upper half, bearing number 5 is a dam bearing with $K' = 3.0$ and $\bar{L}_t = 0.25$. For this case, the stability is increased for the entire range of Sommerfeld numbers compared to the journal bearing. The two separate effects of a pressure dam bearing are shown clearly in Figure 24. The relief track forces the bearing to operate at higher eccentricities, thereby increasing the region of infinite stability. The dam loads up the journal at high Sommerfeld numbers providing a moderate operating eccentricity and higher stability threshold.

The effect of varying the film thickness ratio, K′, on stability was carried out but is not shown here. Reference [14] concludes that the optimum (as far as load capacity is concerned) is approximately K′ = 3.0. A bearing with a film thickness ratio of K′ = 6.0 is only slightly less superior (a 10% decrease at S = 10.0). A 40% decrease in stability is evident for a step bearing with K′ = 12.0 when compared to the K′ = 3.0 bearings at S = 10.0.

The important geometric parameters in pressure dam bearing design are the film thickness ratio, K′ and the dam location, θ_s. Steps should be located at around θ_s = 145° or 150°, while K′ values of between 3.0 and 6.0 are recommended.

From Sommerfeld numbers above S = 2.0, step journal bearings designated with near optimum step location and size can increase the rigid rotor stability parameter, ω_s, by a factor of ten or more over a plain journal bearing. Additionally, the pressure dam bearing would operate at a moderate eccentricity ratio (between ε_b = 0.25 and ε_b = 0.5) even though the loading is light and/or speed high. However, for Sommerfeld numbers below S = 2.0, a step bearing will increase ω_s only slightly (by a factor of around 1.5) over a plain journal bearing even if the optimum dam height and location were used.

Step Bearings on a Single Mass Flexible Rotor

Experimental results are given for different step configurations on similar experimental flexible rotor described in Appendix A. For these tests the rotor was a constant diameter shaft (2.54 cm). A theoretical-experimental comparison of the instability onset speed for the simple flexible rotor is presented [9,15]. Five different step bearing geometries and a two axial groove bearing are considered. The pressure dam bearings employed have different step heights and locations. Optimum and off-optimum designs are used. Instability onset speeds are determined both theoretically and experimentally and a comparison is made to determine the accuracy of the theoretical analysis.

All six pairs of bearings considered have two axial oil supply grooves located at the horizontal split (Figure 22). These grooves are 20° in arc length, making the arc length of both top and bottom pads 160°. The step bearings do not contain a circumferential relief groove in the bottom pad. The two axial groove bearings are identical to the pressure dam design with $h_1 = h_2$ in Figure 22. The length to diameter ratio for each bearing is 1.0 with D = 2.54 cm.

Ideally, each bearing was to have a 5.08 x 10^{-3} cm (2.0 mil) radial clearance. However, due to difficulties in manufacturing, the radial clearance ranged from 4.57 × 10^{-3} to 6.35 × 10^{-3} cm (1.8 to 2.5 mils). The clearance was measured cold with a dial micrometer. Several readings were taken and the average value used.

The important geometric parameters in step bearing design are the film thickness ratio, K′, and the dam location, θ_s. The ratio of film thicknesses is defined as h_1/h_2 when the shaft is centered in the bearing (Figure 22). Thus K′ = h_1/h_2, and K = h_1/c, where h_1 is the centered clearance inside the pocket. The dam location angle, θ_s, is measured with rotation from the positive x (horizontal) axis. Optimum values for favorable stability are around K′ = 3.0 and θ_s = 125° to 150°. Other parameters are the dam axial length ratio $\bar{L}$ = L_d/L (Figure 23) and the relief groove axial length ratio $\bar{L}_t$ = L_t/L. For all cases, L_t = 0.0, since the bottom pad does not have a circumferential relief groove.

A summary of these parameters is listed in Table 5 for all six sets of bearings. Note that step bearing sets 1 and 2 represent the near optimum design with film thickness ratios between 2.1 and 2.8. Sets 3 and 5 are off-optimum designs with larger K′ values between 6.6 and 11.7. The off-optimum angular location is represented by set 4 with θ_s = 90°. The dual numbers in the Table refer to the left (motor) and right ends of the test rotor, respectively.

Figure 25 illustrates the total rotor response with two axial groove bearings. The subsynchronous component first appears at about N = 6600 RPM as the system goes unstable.

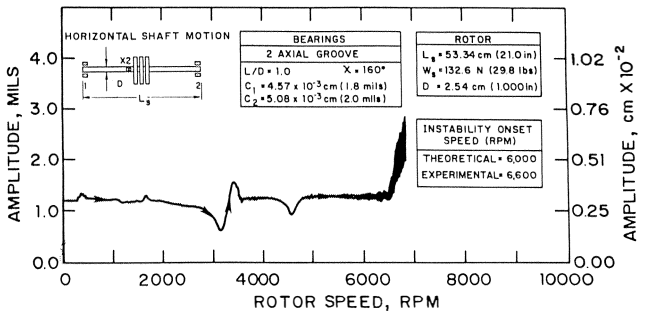

Figure 25. Total Response, Two Axial Groove Bearings.

TABLE 5. SUMMARY OF GEOMETRIC PARAMETERS FOR THE SIX BEARING SETS.

Bearing Set No.	Type	K′	θ_s	c (cm x 10^3)	c (mils)	$\bar{L}_d$
A	Two Axial	1.0	–	4.57	1.8	–
	Groove	1.0	–	5.08	2.0	–
1	Step	2.1	145°	5.59	2.2	0.75
		2.4		6.35	2.5	
2	Step	2.8	140°	6.35	2.5	0.75
		2.6		6.35	2.5	
3	Step	6.6	150°	6.10	2.4	0.75
		8.6		6.35	2.5	
4	Step	3.3	90°	6.10	2.4	0.75
		2.1		6.10	2.4	
5	Step	11.7	140°	5.33	2.1	0.50
		8.3		6.10	2.4	

Common to all bearings: L/D = 1.0, $\bar{L}_t$ = 0.0, χ = 160°

The total response for a near optimum step bearing design (set number 1) is shown in Figure 26 with a corresponding frequency spectrum in Figure 27. This design features a step at θ_s = 145° and film thickness ratios of 2.1 and 2.4. The rotor was run up to maximum speed without a large subsynchronous component appearing. However, two small peaks appear in Figure 26 at around 10,500 RPM and 12,000 RPM. Figure 27 shows a slight nonsynchronous "bump" at 12,000 RPM. It appears that the rotor may be on the instability threshold at 12,000 RPM.

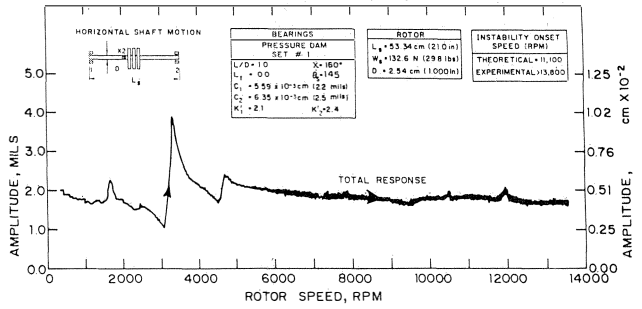

Figure 26. Total Response, Step Bearing Set Number 1, Near Optimum Designs.

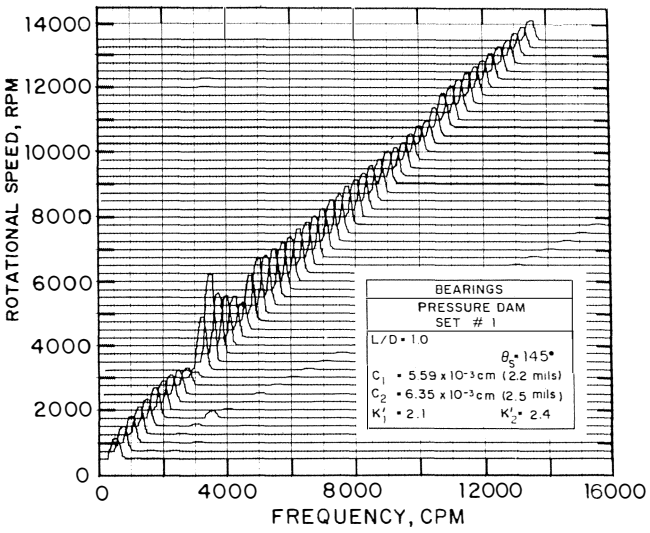

Figure 27. Frequency Spectrum, Step Bearing Number 1, Near Optimum Designs.

An off-optimum design (set number 3) is shown in Figure 28 (speed-amplitude). This design retains the near-optimum θ_s = 150°, but the film thickness ratios are larger with K′ = 6.6 and 8.6. A large synchronous vibration component appears at approximately N = 8900 RPM.

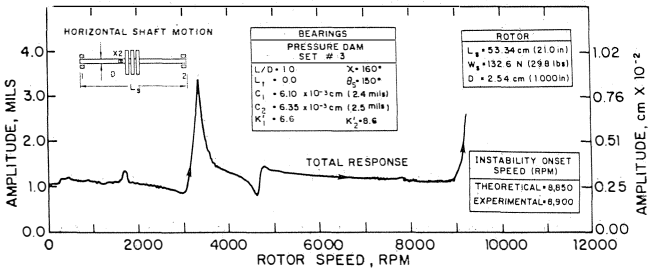

Figure 28. Total Response, Step Bearing Set Number 3, Off-Optimum Film Thickness Ratios.

Table 6 summarizes the experimental results. The near-optimum designs (sets 1 and 2) increase the instability onset speed by 109 and 41 percent, respectively, over the two axial groove bearings. The off-optimum designs (sets 3,4, and 5) increase the instability speed by 35, 30, and 18 percent, respectively.

Comparing step bearing set number 3 to number 5 (increasing the film thickness ratios from 6.6 and 8.6 to 11.7 and 8.3) decreases the instability speed by 12 percent. This trend is somewhat tainted since the dam axial length ratio is smaller for set 5 compared to set 3. Also, the step locations differ by 10°.

To obtain the theoretical instability onset speeds, the stiffness and damping properties of the bearings must be determined. The dynamic properties for all six sets of bearings were calculated using a finite element step bearing computer program that solves the Reynolds equation using finite elements [13]. The same program generated the step bearing characteristic curves in reference [14]. The speed dependent characteristics are used as input data to a stability program that employs a transfer matrix approach similar to the method presented in reference [5].

Table 6 also summarizes the results of the theoretical stability analysis. The experimental results are also indicated alongwith the percent error in the theoretical predictions. The error is under 10 percent for all cases except step bearing sets 1 and 2. Set number 1 has an error greater than 19.6 percent. Set number 2 overestimates the onset speed by 23.7 percent. All other cases theoretically underpredict the instability speed.

TABLE 6. SUMMARY OF THEORETICAL INSTABILITY ONSET SPEEDS FOR THE SIX BEARING DESIGNS.

Bearing Set No.	Type	K^-	θ_s	Instability Onset Speed (RPM) Theoretical	Instability Onset Speed (RPM) Experimental	Percent Error
A	Two Axial Groove	1.0	–	6,000	6,600	9.1%
1	Step	2.1, 2.4	145°	11,100	>13,800	>19.6%
2	Step	2.8, 2.6	140°	11,500	9,300	−23.7%
3*	Step	6.6, 8.6*	150°	8,850	8,900	0.6%
4*	Step	3.3, 2.1	90°*	8,100	8,600	5.8%
5*	Step	11.7, 8.3*	140°	7,800	7,800	0.0%

* Off-optimum

The near-optimum pressure dam bearing designs increase the instability onset speed of the single mass rotor by approximately 109 and 41 percent compared to the two axial groove bearings. Increasing the film thickness ratio from the near-optimum cases decreases the onset speed. Decreasing the step location to 90° from the near-optimum locations also decreases the onset speed.

Pressures have also been measured in step bearings [16] and compared to theoretical predictions. Pressure measurements qualitatively agree with the stability measurements. Namely, sets 1 and 2 produce the largest pressures at the steps, which result in large artificial loads and good stabilizing characteristics.

The theoretical stability analysis predicts the general trends in the experimental data. All step bearing designs increase the onset speed over the two axial groove bearings. The near-optimum designs have the highest onset speeds and the off-optimum designs the lowest.

Side rail construction is important in designing step bearings for optimum stability. Care should be taken to insure uniform pocket depth.

Experimental Step Bearing Stability in a Three Mass Flexible Rotor

In the previous section step bearings were tested with a single mass rotor system. The purpose in this section is to present results for step bearings in the three mass rotor system described in Appendix B.

In Figures 29 and 30 typical results are presented for the rotor in pressure dam bearings #1. These bearings were previously tested with a single mass rotor, and exhibit K′ values very close to the optimum (2.1/2.4). As can be seen in Figure 29, the system becomes unstable at 7400 RPM, again due to whip. The whip frequency is seen in the waterfall diagram, Fig. 30.

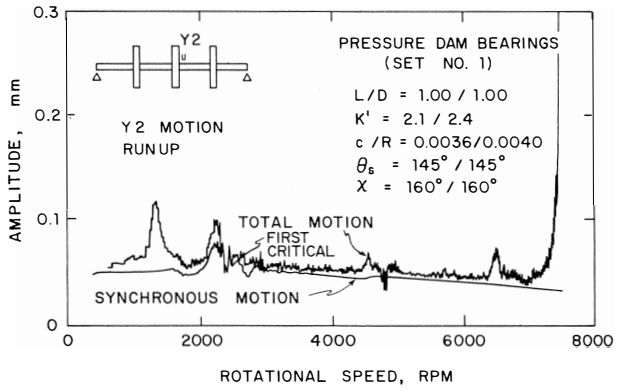

Figure 29. Y2 Response, Rotor in Pressure Dam Bearings #1.

Other step bearings were also tested, but the instability threshold was not changed significantly. Due to the increased flexibilty of the shaft the pressure dam bearings were not able to control the instabilities. The results for the very flexible three mass system indicate that the pressure dam bearings do not significantly improve the system stability as compared to the two axial groove bearings.

In many field applications, if a rotor system is unstable with simple axial groove bearings, one of the common "fixes" is to simply mill a step in the upper half of the bearing. Present

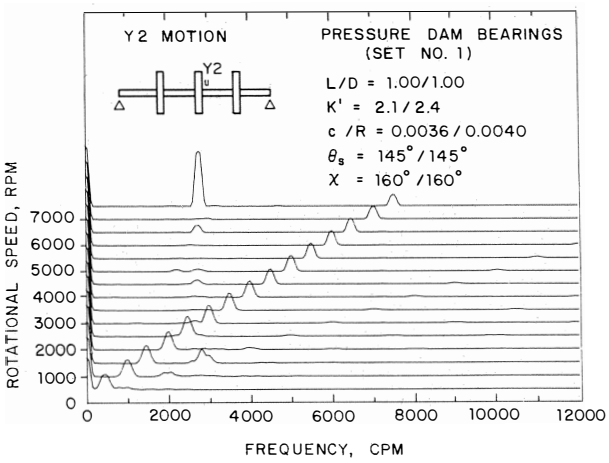

Figure 30. Y2 Waterfall Diagram, Rotor in Pressure Dam Bearings #1.

results indicate that such a procedure will not guarantee machine stability, even for optimum values of K′.

EXPERIMENTAL RESULTS WITH TILTING PAD BEARINGS

This section [15] discusses the same single mass flexible rotor as in previous sections, except that tilting pad bearings are employed. The dimensions are given in Table 7.

TABLE 7. TILTING PAD BEARING SPECIFICATIONS.

Pad Length	22.4 mm
Average Radial Clearance	5.0×10^{-2} mm (2 mils)
Number of pads	five
Pivot angular location	centered
Pad arc length (χ) −	64°
Angle between pads	8°
Pad thickness	762 mm
Preload	0.0
Load orientation	on pad

Figure 31 shows the synchronous and total rotor motion at position X2 on the rotor. The tilting pad bearings exhibited no onset of instability at all up to the maximum speed (10,130 RPM, 1,061 rad/sec) tested. Figure 32 shows the frequency spectrum vs. rotational speed.

A comparison of the data for fixed pad bearings with the tilting pad bearings is instructive. In the horizontal direction, the first critical speed occurs at approximately 2750 RPM (288 rad/sec) upon rotor acceleration regardless of bearing type. Axial groove bearings and pressure dam bearings for this rotor exhibit similarly shaped peaks showing a gradual rise in vibrational level from speeds of 2200 to 3200 RPM (230 to 335 rad/sec). The peak level is approximately 2.8×10^{-3}cm (3.1 mils) for the tilting pad bearings. This indicates greater sensitivity to unbalance at the critical speed for the tilting pad bearings.

On deceleration, the horizontal critical speed occurred at approximately 2850 RPM (298 rad/sec.). The vertical critical

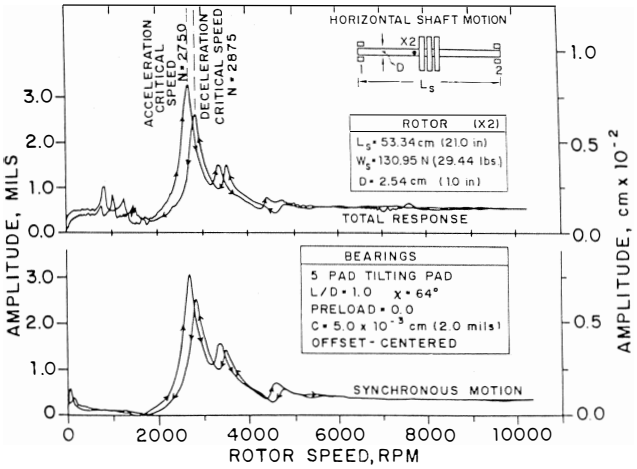

Figure 31. Synchronous and Total Motion — Rotor Mounted in Tilting Pad Bearings (X2 Motion).

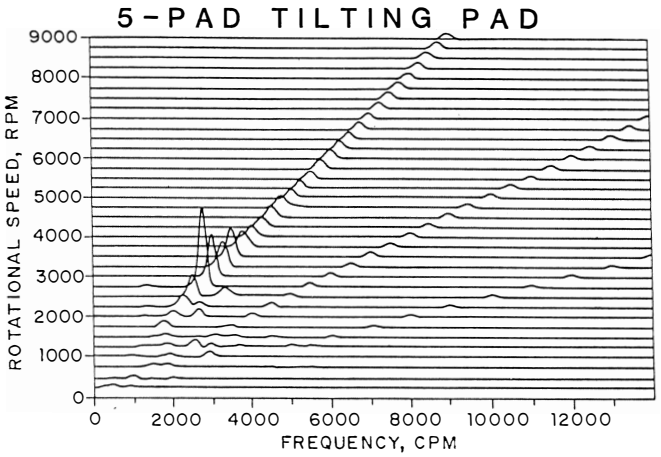

Figure 32. Frequency Spectrum of Vibrational Signal Vs. Rotational Speed for Rotor in Tilting Pad Bearings, Probe Location X2.

speeds were 2925 RPM (306 rad/sec) and 3000 RPM (314 rad/sec) for acceleration and deceleration, respectively.

A secondary critical speed is observed on all plots at approximately half of the rotor natural frequency on run-up. This was due to a misalignment of the coupling from the drive motor. In most cases the amplitude of this peak was greater than the critical frequency peak, but was only observed on acceleration. At either constant speed or on deceleration, there were no abnormal vibration levels observed at this half speed frequency.

Tilting pad bearings do not cause machine instability as do fixed pad bearings. However, the damping in tilting pad bearings may be less effective in suppressing vibrations near a machine critical speed than fixed pad bearings. They may also be incapable of preventing a machine from whirling due to other causes such as aerodynamic cross-coupling or internal friction. Tilting pad bearings are widely used as a cure for bearing induced instability problems — often as a retrofit.

BEARING SUMMARY CHARTS

Table 8 gives some of the advantages and disadvantages of various bearing types in condensed form. The bearing stability or resistance to whirl has been explored in some depth in the earlier sections. Other comments such as "good damping at critical speeds" have come from the authors' experience. The table represents input from many different sources.

In summary, a wide range of bearing designs are available to the designers and users of rotating machinery. These range from very simple plain journal bearings, which are low in cost and easy to make, up to very complex tilting pad bearings which have many components and require very careful design. These can be used to reduce or eliminate vibration problems in many rotating machines. The cost and ease of manufacture must be balanced with the requirements for suppression of non-synchronous vibration in rotating machines.

TABLE 8a. FIXED PAD NON-PRELOADED JOURNAL BEARINGS.

Bearing Type	Advantages	Disadvantages	Comments
Plain Journal	1. Easy to make 2. Low cost	1. Very subject to oil whirl	Round bearings are nearly always "crushed" to make elliptical bearings
Partial Arc	1. Easy to make 2. Low cost 3. Low horsepower loss	1. Poor vibration resistance 2. Oil supply not easily contained	Bearing used only on rather old machines
Axial Groove	1. Easy to make 2. Low cost	1. Subject to oil whirl	Round bearings are nearly always "crushed" to make elliptical or multilobe
Floating Bush	1. Relatively easy to make 2. Low cost	1. Subject to oil whirl	Used primarily in high speed turbochargers for diesel engines in trucks and buses

TABLE 8b. FIXED PAD PRELOADED JOURNAL BEARINGS.

Bearing Type	Advantages	Disadvantages	Comments
Elliptical	1. Easy to make 2. Low cost 3. Good damping at critical speeds	1. Subject to oil whirl at high speeds 2. Load direction must be known	Probably most widely used bearing at low or moderate speeds
Offset Half (With Horizontal Split)	1. Excellent suppression of whirl at high speeds 2. Low cost 3. Easy to make	1. Fair suppression of whirl at moderate speeds 2. Load direction must be known	Has high horizontal stiffness and low vertical stiffness — may become popular — used outside U.S.
Three- and Four-Lobe	1. Good suppression of whirl 2. Overall good performance 3. Moderate cost	1. Some types can be expensive to make properly 2. Subject to whirl at high speeds 3. Goes unstable with little warning 4. Very high vibration levels during instability	Currently used by some manufacturers as standard bearing design

TABLE 8c. FIXED PAD JOURNAL BEARINGS WITH STEPS, DAMS, OR POCKETS.

Bearing Type	Advantages	Disadvantages	Comments
Pressure Dam (Single Dam	1. Good supression of whirl 2. Low cost 3. Good damping at critical speeds 4. Easy to make	1. Goes unstable with little warning 2. Dam may be subject to wear or build-up over time 3. Load direction must be known 4. Does not suppress whirl for very flexible rotors	Very popular with petrochemical industry. Easy to convert elliptical over to pressure dam
Multi Dam Axial Groove or Multilobe	1. Dams are relatively easy to place in existing bearings 2. Good suppression of whirl 3. Relatively low cost 4. Good overall performance	1. Complex bearing requiring detailed analysis 2. May not suppress whirl due to non-bearing causes	Used as standard design by some manufacturers
Hydrostatic	1. Wide range of design parameter 2. Moderate cost 3. Good load capacity of low speeds	1. Poor damping at critical speeds 2. Requires careful design 3. Requires high pressure lubricant supply	Generally high stiffness properties used for high precision rotors

TABLE 8d. NONFIXED PAD JOURNAL BEARING.

Bearing Type	Advantages	Disadvantages	Comments
Tilting Pad	1. Will not cause whirl (no cross-coupling) 2. Wide range of design parameters 3. Original cost about the same as other bearings	1. High replacement cost 2. Requires careful design 3. Poor damping at critical speeds 4. Hard to determine actual clearances 5. High horsepower loss	Widely used bearing to stabilize machines with synchronous non-bearing excitations

ACKNOWLEDGEMENTS

The work described in this paper has largely been published elsewhere as indicated in the references. This paper is intended as a sampler of different works carried out for several bearing types in order to provide an introduction to bearing design for the user of turbumachinery.

Various phases of the work reported in this paper have been supported in part by U.S. Department of Energy Contract No. DE-ACO1-79ET-13151, NASA Lewis Research Contract No. NSG-3177-1 and Engineering Foundation Grant No. RC-A-77-6C. The authors also acknowledge support from the Industrial Supported Program for the Dynamic Analysis of Turbomachinery and the Rotating Machinery and Controls (ROMAC) Industrial Research Program, both at the University of Virginia.

REFERENCES

1. Gunter, E. J., Barrett, L. E., and Allaire, P. E., "Design and Application of Squeeze Film Dampers for Turbomachinery Stabilization," *Proceedings of the Fourth Turbomachinery Symposium,* Texas A&M University, College Station, Texas, 1975, pp. 89-118.
2. Allaire, P. E., and Flack, R. D., "Journal Bearing Design for High Speed Rotating Machinery," Invited paper presented at 1980 ASME-ASLE International Lubrication Conference, August 18-21, 1980, San Francisco, California, in *Bearing Design—Historical Aspects, Present Technology, and Future Problems,* ASME publication No. H00160, pp. 111-159.
3. Li, D. F., Choy, K. C., and Allaire, P. E., "Stability and Transient Characteristics of Four Multilobe Journal Bearing Configurations," *Journal of Lubrication Technology,* Trans. ASME, Vol. 102, No. 3 (July, 1980), pp. 291-299.
4. Leader, M. E., Flack, R. D., and Lewis, D. W., "An Experimental Determination of the Instability of a Flexible Rotor in Four-Lobe Bearings," *Wear,* Vol. 58. No. 1 (1980), pp. 35-47.
5. Lund, J W., "Stability and Damped Critical Speeds of a Flexible Rotor in Fluid-Film Bearings," *Journal of Engineering for Industry,* Trans. ASME, Vol. 96, No. 2 (May 1974), pp. 509-517.
6. Lanes, R. F., Flack, R. D., and Lewis, D. W., "Experiments on the Stability and Response of a Flexible Rotor in Three Types of Journal Bearings," accepted for publication in *ASLE Transactions,* in press, Preprint No. 81-AM-2E-2.
7. Lanes, R. F., and Flack, R. D., "Effects of Three Lobe Bearing Geometries on Flexible Rotor Stability," accepted for publication in *ASLE Transactions,* in press.
8. Flack, R. D., and Lanes, R. F., "Effects of Three Lobe Bearing Geometries on Rigid Rotor Stability," accepted for publication in *ASLE Transactions,* in press, Preprint No.81-AM-2E-1.
9. Nicholas, J. C., Barrett, L. E., and Leader, M. E., "Experimental-Theoretical Comparison of Instability Onset Speeds for a Three Mass Rotor Supported by Step Journal Bearings," *Journal of Mechanical Design,* Trans. ASME, Vol. 102, No. 2 (April 1980), pp. 334-351.
10. Flack, R. D., Leader, M. E., and Allaire, P. E., "An Experimental and Theoretical Investigation of Pressures in Four-Lobe Bearings," *Wear,* Vol. 61, No. 2 (June 16, 1980), pp. 233-242.
11. Flack, R. D., and Allaire, P. E., "An Experimental and Theoretical Examination of the Static Characteristics of Three-Lobe Bearings," accepted for publication in *ASLE Transactions,* in press, Preprint No. 80-LC-7C-1.
12. Allaire, P. E., Nicholas, J. C., and Barrett, L. E., "Analysis of Step Journal Bearings — Infinite Length, Inertia Effects," *ASLE Trans.,* Vol. 22, No. 4 (October, 1979), pp. 333-341.
13. Nicholas, J. C., and Allaire, P. E., "Analysis of Step Journal Bearings — Finite Length, Stability," *ASLE Trans.,* Vol. 23, No. 2 (April, 1980), pp. 197-207.
14. Nicholas, J. C., Allaire, P. E., and Lewis, D. W., "Stiffness and Damping Coefficients for Finite Length Step Journal Bearings," *ASLE Trans.,* Vol. 23, No. 4 (October, 1980), pp. 353-362.
15. Leader, M. E., Flack, R. D., and Allaire, P. E., "Experimental Study of Three Journal Bearings with a Flexible Rotor," *ASLE Trans.,* Vol. 23, No. 4 (October, 1980), pp. 363.
16. Flack, R. E., Leader, M. E., and Allaire, P. E., "Experimental and Theoretical Pressures in Step Journal Bearings," *ASLE Trans.,* Vol. 24, No. 3 (July 1981), pp. 316-322.

APPENDIX A

SINGLE MASS FLEXIBLE ROTOR EXPERIMENTAL APPARATUS

The Test Rotor

The test rotor consists of a flexible shaft with three closely mounted disks located midway between two bearing supports (Figure A-1). The combined weight of the shaft and central masses is 13.35 kg. The three masses were mounted onto the shaft by means of a cone and neoprene "O" ring which securely fastened the disks to the shaft without adding any appreciable stiffness. Each disk has 24 balance holes, each 15° apart. The three disks were mounted such that successive balance holes were incremented by 5°. The shaft was nominally 2.54 cm in diameter with 2.22 cm diameter undercuttings such that the disks could be removed or moved easily. This rotor system has a first rotor critical speed of 3000 RPM.

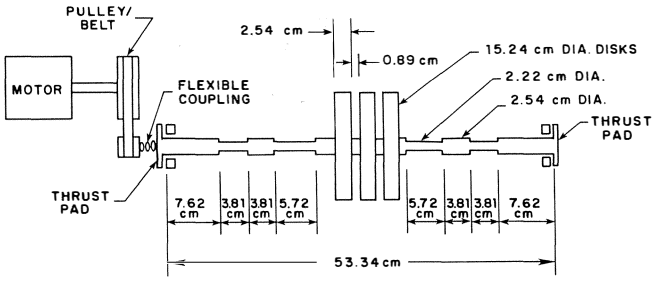

Figure A-1. Shaft and Motor Assembly.

The rotor is driven by a one horsepower DC motor through a belt/pulley and flexible coupling. A pulley ratio of 5.65 was used and the maximum speed of the motor is approximately 2400 RPM. The torque and speed of the system are electronically controlled and operator adjustable. Any rotor speed between 100 and 13,000 RPM can be obtained and held

within one RPM. The misalignment of bearings with respect to the shaft is known to affect the response of a rotor-bearing system, particularly for multilobe bearings. Thus, the flexible coupling as shown in Figure A-1 was used to minimize this effect.

The interchangeable bearings are mounted in pedestals on top of an oil filled and temperature controlled reservoir. The entire apparatus is clamped to a 900 kg concrete foundation for vibration isolation. The oil (Shell automotive type 10W-20W-50) was heated to 54°C and fed at low oil pressure (approximately 20.7 KPa) to the bearing surfaces through the oil feed grooves. At this temperature, the dynamic viscosity was measured to be 50 cP with a viscometer. The viscosity was also measured to be 195 cP and 35.5 cP at 30°C and 70°C, respectively. The two bearings had thrust pads as shown in Figure A-1 to restrict the axial motion of the rotor.

Instrumentation

Shaft vibrational motion was monitored by eight noncontacting probes mounted in aluminum shells at four locations (Figure A-2). A standard right-hand coordinate system is employed to facilitate comparison to mathematical analysis and computer modeling. The raw signal from each probe was passed through a coaxial cable to an oscillator/demodulator and then to the synchronous tracking filter. Each probe-oscillator/demodulator combination was calibrated for linearity and chosen such that the response of the probes were matched. Thus, direct comparison of the outputs of the various probes was possible. In addition to the vibration pick-ups, a proximity probe was placed over a notch in the shaft on the x-axis as a zero degree reference for balancing and to monitor rotational speed.

The synchronous tracking filter has outputs to display the synchronous and total vibration orbits on the oscilloscope as well as speed and amplitude of vibration outputs for use with the x-y recorder. The phase angle of the synchronous orbit was also plotted against speed. Vibration amplitude was plotted against RPM for each bearing station and for each orientation of the bearing.

Before each test, the rotor was balanced at the rotor first critical speed using the three trial weight method. A small residual unbalance resulted from this balance technique. The shaft had a bow vector of approximately 0.015 mm. The accuracy range for the method is ± 7 gm-cm.

Two test runs were made for each bearing configuration. For the first, the speed of the rotor was increased at the maximum acceleration until the stability threshold was attained, at which time the power was shut off and the rotor was allowed to coast to a stop. The average acceleration and deceleration rates were 15 rad/sec^2 and −8 rad/sec^2, respectively. For the second tests, the speed of the rotor was increased incrementally (typically by 500 RPM) so that the rotor ran for approximately 30 sec at the constant speed plateaus. During the tests, the motion of the rotor was carefully monitored by using the synchronous tracking filter. The data was also recorded by a fourteen channel FM tape recorder such that the data could be further analyzed after the tests.

After the tests the data was reduced by two methods. First, both the synchronous and total (synchronous + asynchronous) amplitudes of the motion at various locations were plotted as a function of the rotor speed using the synchronous tracking filter and the data from the first test. The phase of the synchronous motion was also plotted.

From the second set of data waterfall of "cascade" frequency, spectrum plots were constructed. A fast Fourier transform digital signal analyzer was used to obtain frequency spectrums at the constant speed plateaus. By plotting the spectrums vertically and equally spaced, the "cascade" plots were obtained. Overall, the instrumentation used in this investigation is summarized in Figure A-3.

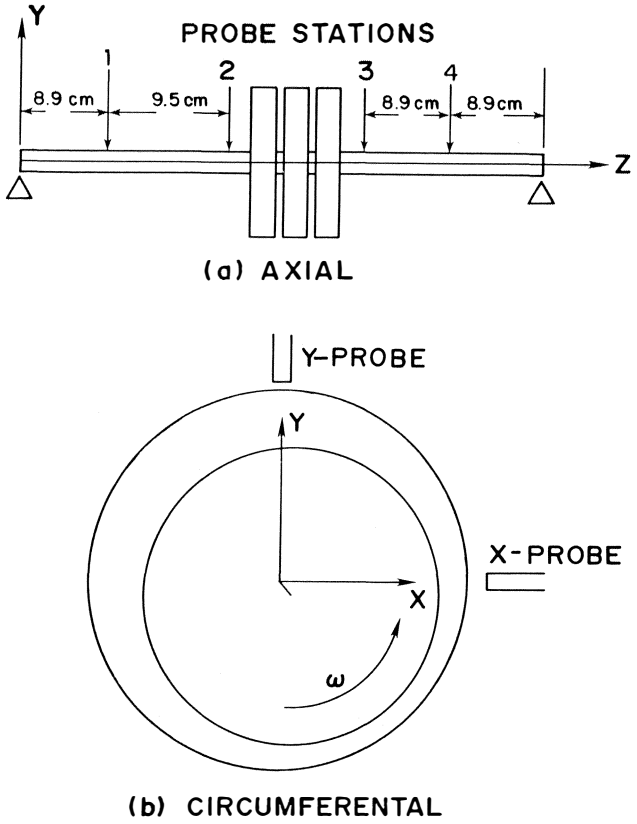

Figure A-2. Noncontacting Probe Locations.

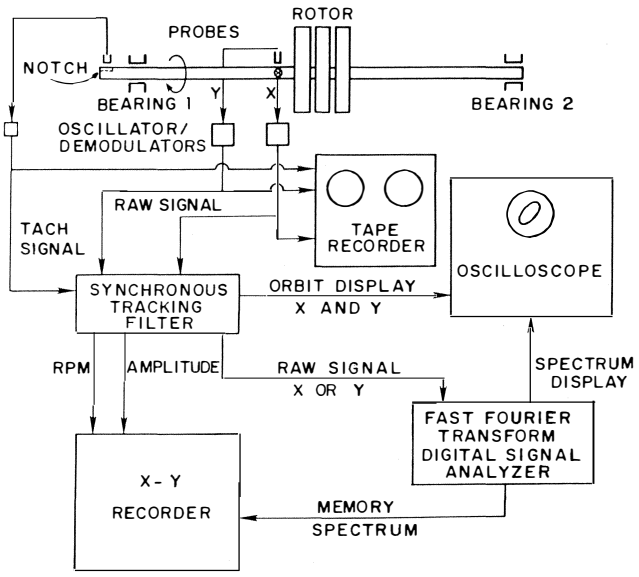

Figure A-3. Instrumentation for Test Rotor.

APPENDIX B

THREE MASS FLEXIBLE ROTOR APPARATUS

In this Appendix the three mass flexible rotor is described. The rig is nearly identical to that described in Appendix A with the exception of the shaft diameter and mass locations. The instrumentation to reduce the data is identical. The specifications are shown in Figure B-1.

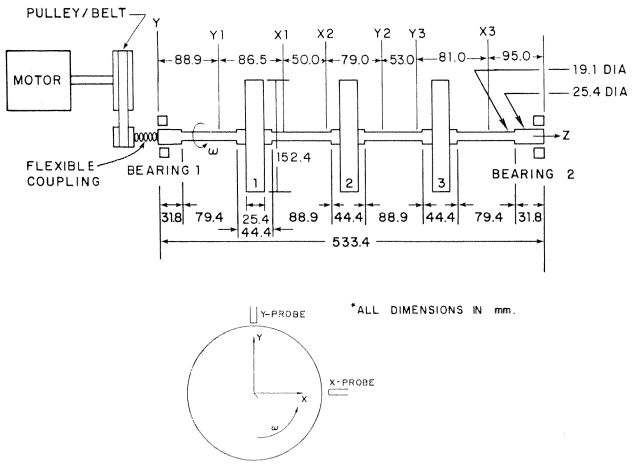

Figure B-1. Rotor Dimensions and Probe Locations.

NOMENCLATURE

Dimensional Quantities

c, c_1, c_2 = Bearing radial clearance, number one bearing, number two bearing (L)

c_b = Minimum film thickness for a centered shaft (L)

c_d = Step height (L)

c_p = Lobe clearance (L)

$C_{xx}, C_{xy}, C_{yx}, C_{yy}$ = Bearing damping coefficients (FTL^{-1})

D = Bearing diameter (L)

e = Bearing eccentricity (L)

F_x, F_y = Bearing forces in the x and y directions (F)

g = Gravitational acceleration (L/T^2)

h_1, h_2 = Film thickness before, after step, centered bearing ($h_2 = c$) (L)

$K_{xx}, K_{xy}, K_{yx}, K_{yy}$ = Bearing stiffness coefficients (FL^{-1})

$K' \cdot$ = $\dfrac{h_1}{h_2} = \dfrac{h_1}{c}$, Film thickness ratio

L = Bearing length (L)

L_d, L_t = Step bearing axial dam length, relief track axial length (L)

m, m' = Rotor mass (M)

N, N_s = Shaft rotational speed (RPM), (RPS)

O_b, O_j, O_p = Bearing, journal, pad, center

R = Radius of shaft (journal) (L)

R_p = Lobe radius (L)

W, W_T = Static bearing load (F)

x, y = Journal position in the x and y coordinates (L)

$\dot{x}, \dot{y}$ = Journal velocity in the x and y coordinates (L/T)

$\ddot{x}, \ddot{y}$ = Journal acceleration in the x and y coordinates (L/T^2)

γ_g = Groove location, (degrees)

δ = Pad tilt angle (degrees)

μ = Fluid viscosity (FT/L^2)

ω_d = Rotor whirl frequency (1/T)

ω_j = Journal rotational speed (1/T)

ω_r = Rotor critical speed on rigid support (1/T)

θ_g = Groove location, (degrees)

θ_s = Location of step measured with rotation from positive x-axis (degrees)

χ = Lobe arc length

Non-Dimensional Quantities

$\bar{C}_{xx}, \bar{C}_{xy}, \bar{C}_{yx}, \bar{C}_{yy}$ = Dimensional damping coefficients, $\bar{C}_{xx} = C_{xx}(\omega_j c/W_T)$

$\bar{K}_{xx}, \bar{K}_{xy}, \bar{K}_{yx}, \bar{K}_{yy}$ = Dimensional stiffness coefficients, $\bar{K}_{xx} = K_{xx}(c/W_T)$

$\bar{L}_d, \bar{L}_t$ = L_x/L, L_t/L, Step bearing axial dam length ratio, relief track axial length ratio

m_1, m_2 = Preload in multilobe bearings

$\bar{M}$ = Rotor mass, $\omega_j^2 cm/W$

Re_2 = Reynolds number for step bearing

S = $\dfrac{\mu N_s L D}{W_T}\left(\dfrac{R}{c}\right)^2$, Sommerfeld number

S' = $\dfrac{\mu N_s L D}{W_T}\left(\dfrac{R}{c_b}\right)^2$, Sommerfeld number

η = Bearing parameter,

$$\mu L D \left(\frac{D}{c}\right)^2 \left(\frac{W}{cm}\right)^{1/2} \Big/ 8\pi W$$

$\bar{\omega}_d$ = Whirl frequency ratio, ω_d/ω_j

$\bar{\omega}_j$ = Rotor speed parameter, $\omega_j \sqrt{mc/W}$

ω_s = $\omega_j \sqrt{c/g}$, Rotor speed parameter, horizontal rotor

ω_s = $\omega_j \sqrt{\dfrac{m\ c}{W_T}}$, Rotor speed parameter

ω_s = Rigid rotor stability threshold

ω_s = Flexible rotor stability threshold

α = Offset factor

ε = e/c_b, Bearing eccentricity ratio

Subscripts

b = Bearing

d = Dam

g = Groove

j = Journal

max = Maximum magnitude

p = Pad or lobe

r = Relative to equilibrium position
s = Step
t = track
x,y = Horizontal and vertical directions
1,2 = Bearings 1 and 2 in experimental rotor